

Are Starburst Galaxies Proton Calorimeters?

Xilu Wang

and

Brian D. Fields¹

Department of Astronomy, University of Illinois, Urbana, IL 61801, USA

`xwang107@illinois.edu, bdfields@illinois.edu`

ABSTRACT

Several starburst galaxies have been observed in the GeV and TeV bands; in this regime, gamma-rays are mainly produced through the pionic process from cosmic-ray proton interactions with the interstellar medium ($p_{\text{cr}}p_{\text{ism}} \rightarrow \pi^0 \rightarrow \gamma\gamma$). Furthermore, the dense environments of starbursts have been proposed to act as proton “calorimeters” in which collisions dominate proton losses, so that a substantial fraction of cosmic-ray proton energy inputs is emitted in gamma rays. Here we build a one-zone, “thick-target” model that implements calorimetry and thus places a firm upper bound to the gamma-ray emission due to cosmic-ray interactions. The model assumes that cosmic rays are accelerated by supernovae, and escape is neglected. Both inelastic and elastic nuclear interactions of the cosmic rays are included self-consistently. Our model has only two free parameters: the cosmic-ray proton acceleration energy per supernova ϵ_{cr} , and the proton injection spectral index s . We find that in the thick-target limit, the emergent gamma-ray spectral index is the same as the injection index s , and not that of the propagated cosmic rays. We calculate the pionic gamma-ray emission from 10 MeV to 10 TeV for five starburst galaxies (M82, NGC253, NGC4945, NGC1068 and Circinus) and the ultraluminous infrared galaxy Arp220. Using *Fermi*, *H.E.S.S.*, and *VERITAS* data, we perform chi-squared fits to derive best-fit thick-target parameters for each galaxies. We find that the model provides good fits for the best-observed galaxies M82 and NGC253, with cosmic-ray acceleration energetics and spectral indices that are consistent with both theoretical expectations and *Fermi* observations of Galactic supernova remnants; this suggests that cosmic-ray acceleration and injection by supernovae is similar in starbursts and in our Galaxy. Turning to cosmic-ray propagation after injection, we find that these starbursts are indeed nearly if not fully proton calorimeters, in contrast to the Mikly Way. For NGC4945 and NGC1068, the models are not well-constrained due to the lack of TeV data, but the GeV data also are consistent with near or full proton calorimetry. Consequently, we conclude that these starbursts, and

¹also Department of Physics, University of Illinois

perhaps most starbursts, are consistent with near or total proton calorimetry. Finally, we find that both Arp220 and the Circinus galaxy lie above our pionic upper-limit, suggesting these objects harbor other gamma-ray sources, or supernovae that are substantially more efficient accelerators, or that their supernova rates are underestimated by their far-infrared luminosities.

Subject headings: gamma rays: galaxies, galaxies: starburst, (ISM:) cosmic rays

1. Introduction

Cosmic rays (CRs) are accelerated by supernovae (e.g., Baade & Zwicky 1934; Ginzburg & Syrovatskii 1964; Ackermann et al. 2013), and thus cosmic-ray production is an inevitable consequence of star formation. As CRs propagate in the interstellar medium (ISM), inelastic collisions between CR and interstellar nuclei—both dominantly protons—lead to gamma-ray production via π^0 decay: $p_{\text{cr}}p_{\text{ism}} \rightarrow \pi^0 \rightarrow \gamma\gamma$ (Stecker 1971; Dermer 1986). This process occurs not only in the Milky Way, but also in other star-forming galaxies (e.g., Dermer 1986; Strong et al. 1976; Lichti et al. 1978; Pavlidou & Fields 2001; Stecker & Venters 2011; Abdo et al. 2009; Fields et al. 2010; Strong et al. 2010). Thus, cosmic-rays are both qualitatively and quantitatively probed by gamma-rays from star-forming galaxies.

Starburst galaxies are a particularly interesting class of star-forming galaxies. Compared with normal galaxies like Milky Way, starbursts and ultraluminous infrared galaxies (ULIRGs, the very extreme starbursts) have exceptionally high star-formation rates and harbor regions of very dense gas. Thus cosmic rays accelerated in starbursts are expected to be lost due to interaction rather than escape, whereas normal star-forming galaxies are in the opposite regime. In the limit where all of the CR nuclei interact with ISM rather than escape, a large fraction of initial proton energy is emitted as gamma rays, making such a galaxy a “proton calorimeter” (e.g., Pohl 1993, 1994; Lacki et al. 2011; Abramowski et al. 2012).¹ This situation has the maximum efficiency to convert supernova blast energy into gamma rays. Therefore the starbursts galaxies were anticipated to be detected as gamma-ray sources (e.g., Paglione et al. 1996; Blom et al. 1999; Domingo-Santamaría & Torres 2005; Persic et al. 2008; de Cea del Pozo et al. 2009; Rephaeli et al. 2010).

Fermi LAT is the first gamma-ray telescope to observe the starburst galaxies, and is also the first one to study external star-forming galaxies as a population. Three of the *Fermi* detections are normal star-forming galaxies: the Large Magellanic Cloud (LMC Abdo et al. 2010), the Small Magellanic Cloud (SMC Abdo et al. 2010), and M31 (Abdo et al. 2010). Five additional *Fermi* detections are starburst galaxies: M82 and NGC253 (Abdo et al. 2010), NGC4945 and NGC1068 (Nolan et al. 2012), as well as the Circinus galaxy (Hayashida et al. 2013). The

¹ A closely analogous concept is cosmic-ray electron calorimetry, as suggested observationally by, e.g., the far infrared–radio correlation (e.g., Voelk 1989).

two nearest and brightest starbursts, M82 and NGC253, are also detected at TeV energies by *VERITAS* (Acciari et al. 2009) and *H.E.S.S.* (Acero et al. 2009; Abramowski et al. 2012), respectively. Peng et al. (2016) and Griffin et al. (2016) recently reported *Fermi* detections of the ULIRG Arp220. Star-forming galaxies represent a new gamma-ray source class, and offer unique insight into the global behavior of cosmic rays over a wide range of galaxy types and star-formation rates.

Various models have been built for starbursts to study the multi-frequency emissions from radio to γ -rays, considering both hadronic and leptonic processes (e.g., synchrotron radiation, inverse Compton scattering, pion production). For example, Blom et al. (1999), Persic et al. (2008), de Cea del Pozo et al. (2009), Lacki et al. (2011), Lacki et al. (2012), Paglione & Abrahams (2012), Yoast-Hull et al. (2013) give their predictions of gamma-radiation from M82, while NGC253 are anticipated to be observed in GeV-TeV range by Paglione et al. (1996), Domingo-Santamaría & Torres (2005), Rephaeli et al. (2010), Lacki et al. (2011); Lacki et al. (2012), Paglione & Abrahams (2012), Yoast-Hull et al. (2014). Recent observations and current theoretical models of starbursts are also reviewed by Ohm (2016). Many-but not all-of these models predict that hadronic processes dominate above a few GeV. In this paper, our aim is to calculate self-consistently the pionic emission from starbursts in a closed box, and to use starburst data to test this calorimetric scenario. By construction, our more focused model is economical and thus easy to test: it contains only two parameters, the cosmic-ray acceleration energy per supernova ϵ_{cr} , and the cosmic-ray injection index s . Some early results from our calculations were summarized in Wang & Fields (2014) and Wang & Fields (2016).

The next section shows the assumptions, important expressions and physics of our thick-target model. An order of magnitude estimation of the pionic gamma-ray luminosity of individual starbursts are presented in § 2. § 4 presented the results calculated from our model when applying to five observed starbursts galaxies. In § 5, further discussions and conclusions are given.

2. The Thick-Target/Calorimetric Model

To calculate the hadronic gamma-ray output in our model, we first characterize the cosmic-ray sources and their thick-target propagation. We then use the propagated cosmic-ray flux to arrive at hadronic gamma-ray emission. The calculation in this section adopts GeV as the energy unit.

2.1. Cosmic-Ray Source and Propagation

We describe the production and propagation of cosmic rays in a one-zone, thick-target “closed-box” model that has the following basic assumptions: 1) cosmic-rays and ISM gas are both spatially homogeneous; 2) cosmic rays are accelerated by supernovae (SNe) with acceleration energy per SN ϵ_{cr} ; 3) the injected cosmic-ray/proton spectrum is a power law in momentum, of spectral index s in GeV and TeV energy range; 4) all the cosmic rays will interact with ISM, i.e. the escape rate

of protons is zero; 5) among the gamma-ray production mechanisms, pion production and decay dominates. The physical processes in our model are CR ion accelerated by SNe, pion production through the interaction between CR and ISM and the following neutral pion decay is responsible for the existing gamma-rays.

Starting from the general propagation equation (e.g., Longair 1981; Strong et al. 2007; Meneguzzi et al. 1971; Fields et al. 1994), we can get the propagation equation for cosmic rays to be

$$\partial_t N_E = \partial_E (b_E N_E) - \frac{1}{\tau_E} N_E + q_E \quad . \quad (1)$$

Here and throughout, E denotes *kinetic* energy per nucleon, and $N_E dE$ is the number density of cosmic rays with kinetic energy $\in (E, E + dE)$. In eq. (1), τ_E is the lifetime of cosmic ray against escape, q_E is the injected cosmic ray spectrum, $b_E = -dE/dt$ is the rate of energy loss (per nucleon). We assume a closed-box, with no escape of cosmic rays, hence $1/\tau_E = 0$. The cosmic-ray density then approaches a steady state solution, $\partial_t N_E = 0$, over the energy loss timescale $\int dE/b \sim E/b$. The closed-box, steady-state solution to eq. (1) then becomes:

$$N_E = \frac{dN}{dV dE} = -\frac{q(> E)}{b(n_{\text{gas}}, E)} = -\frac{\int_E^\infty q_{E'} dE'}{b(n_{\text{gas}}, E)} \quad (2)$$

The cosmic-ray number flux is $\phi(E) = v_E N_E$, with v_E the velocity at E , and so the propagated steady-state proton flux is

$$\phi_p(E) = v N_E = \frac{v_p}{b(n_{\text{gas}}, E)} \int_E^\infty dE' q_E(E') \quad (3)$$

where n_{gas} is the atomic hydrogen density of the interstellar medium. We see that in this simple model, the cosmic-ray flux depends only the cosmic ray source function q_E and energy loss rate b .

Since cosmic rays accelerated by the supernovae in our model, energy conservation :

$$L_{\text{cr}} = \frac{dE_{\text{cr}}}{dt} = E_{\text{sn}} f_{\text{cr}} R_{\text{sn}} = \epsilon_{\text{cr}} R_{\text{sn}} = V \int_{E_{\text{min}}}^\infty E \frac{dq}{dp} dp \quad (4)$$

where L_{cr} is the injected cosmic ray luminosity, V is the volume of the galaxy where cosmic-ray is produced, E_{min} is the minimum kinetic energy of injected protons which can be accelerated. E_{sn} is the total baryonic energy released by one SN explosion. Some fraction f_{cr} of this explosion energy goes to accelerate cosmic rays, and this leads to the other free parameter in our model: $\epsilon_{\text{cr}} = E_{\text{sn}} f_{\text{cr}}$ the cosmic-ray proton acceleration energy per supernova. R_{sn} is SN rate, which can be converted from the star formation rate (SFR) ψ by $R_{\text{sn}}/\psi \sim 0.00914 M_\odot^{-1}$ (Lien & Fields 2009).

Following the simplest (i.e., test particle) expectations of diffusive shock acceleration (e.g., Krymskii 1977; Bell 1978; Blandford & Ostriker 1978) we assume the injected cosmic ray spectrum (emissivity) is a power law in momentum:

$$q_p = \frac{dN}{dV dt dp} = \frac{dq}{dp} = \frac{q_0}{I} p^{-s} \quad (5)$$

where $q_0 = L_{\text{cr}} V$ is the cosmic ray luminosity density, I is the normalization factor, s , the proton spectral injection index, is a free parameter in the model (> 2.0). See §4.2 for more discussion of this assumption.

Finally we can get the accelerated proton spectrum:

$$\phi_p(E) = \frac{q_0 v_p}{I b(n_{\text{gas}}, E)} \frac{(p_p)^{1-s}}{s-1} \quad (6)$$

where p_p is proton's momentum, and I is a number which is determined by E_{min} : $I = I(E_{\text{min}}) = \int_{E_{\text{min}}}^{\infty} E \cdot (E + m_p) \cdot (p_p)^{-s-1} d(E)$, m_p is the mass of proton.

2.2. Pionic Emission From Thick-Target Galaxies: the Calorimetric Model

Our notation and approach follows that of Dermer (1986). From the accelerated proton spectrum, we can get pion's spectrum (in the lab frame) through the interaction $p_{\text{cr}} p_{\text{ism}} \rightarrow \pi^0 \rightarrow \gamma\gamma$:

$$\frac{dq_{\pi}(E_{\pi})}{dE_{\pi}} = n_{\text{gas}} \int_{E_p^{\text{threshold}}}^{\infty} dE_p \cdot \phi_p(E_p) \cdot \frac{d\sigma_{\pi}(E_{\pi}, E_p)}{dE_{\pi}} \quad (7)$$

In turn, the gamma-ray spectrum is

$$\frac{dq_{\gamma}(E_{\gamma})}{dE_{\gamma}} [\text{photons}/(\text{cm}^3 - \text{s} - \text{GeV})] = 2 \int_{E_{\gamma} + (m_{\pi}^2/4E_{\gamma}) - m_{\pi}}^{\infty} dE_{\pi} \cdot \frac{dq_{\pi}(E_{\pi})/dE_{\pi}}{((E_{\pi} + m_{\pi})^2 - m_{\pi}^2)^{1/2}} \quad (8)$$

where $E_p^{\text{threshold}}(E_{\pi})$ is the threshold proton kinetic energy which can produce a pion with energy. m_p is the mass of neutral pion. $d\sigma_{\pi}(E_p, E_{\pi})/dE_{\pi}$ is the differential cross section for the production of a π^0 with energy E_{π} , which can be written as $d\sigma_{\pi}(E_p, E_{\pi})/dE_{\pi} = \langle \zeta \sigma_{\pi}(E_p) \rangle dN(E_p, E_{\pi})/dE_{\pi}$, $\langle \zeta \sigma_{\pi}(E_p) \rangle$ is the inclusive cross section for the reaction $p_{\text{cr}} p_{\text{ism}} \rightarrow \pi^0 \rightarrow \gamma\gamma$.

Our model is self-consistent by calculating the inelastic energy loss from cross-section $\langle \zeta \sigma_{\pi}(T_p) \rangle$. Here we use Dermer (1986)'s fit to the inclusive π^0 data in p-p reaction for the neutral pionic inclusive cross-section $\langle \zeta \sigma_{\pi}(E_p) \rangle$, and thus we can get the inelastic energy loss rate consistently (assuming the loss is approximated to be continuous):

$$b_{\text{inelastic}} = 3 \cdot n_{\text{gas}} \cdot v_p \cdot \langle \zeta \sigma_{\pi}(E_p) \rangle \cdot \int_0^{E_p} E_{\pi} dN(E_p, E_{\pi})/dE_{\pi} dE_{\pi}. \quad (9)$$

The crucial factor of 3 here comes from assuming the inclusive cross sections for $p_{\text{cr}} p_{\text{ism}} \rightarrow \pi^{\pm} + \text{anything}$ are the same as π^0 , i.e., the production rates for (π^-, π^0, π^+) are approximately the same. This factor of 3 has a direct impact on the gamma-ray production efficiency: the gamma energy output per energy into CRs above pionic threshold would be 1/3 if the inelastic losses were the only ones. The efficiency will be lower still when also including CRs below the pionic threshold, and when including other CR losses, to which we now turn.

We also include the energy loss contributions due to nuclear elastic scattering (Gould 1982) and ionization (Ginzburg & Syrovatskii 1964): $b(n_{\text{gas}}, E) = b_{\text{inelastic}} + b_{\text{elastic}} + b_{\text{ioniz}}$, with rates given in the AppendixA. These two terms also affect the gamma-ray production efficiency: ionization loss is only important at low energies, but the elastic scattering is important at all energies and in general is comparable to inelastic. Thus elastic losses are the more important to lower the CR efficiency.

The function $dN(E_p, E_\pi)/dT_\pi$ encodes the distribution of pion energies at each proton energy. We adopt Dermer (1986)’s approach, combining Stecker’s isobaric model (model S, Stecker 1970) together with Stephens and Badhwar’s scaling model (model SB, Stephens & Badhwar 1981): for $E_p < 3\text{GeV}$, model S is used; while model SB is adopted for $E_p > 7\text{GeV}$; for $3\text{GeV} < E_p < 7\text{GeV}$, model S and model SB is linearly connected to be used.

Putting the expressions together, we can get the final equation for the gamma-ray spectrum to be:

$$\begin{aligned} \frac{dq_\gamma}{dE_\gamma} &= \frac{dN_\gamma}{dV dE_\gamma dt} \\ &= \frac{\epsilon_{\text{cr}} R_{\text{sn}}}{VI(E_{\text{min}})} I_0(E_\gamma, s) \end{aligned} \quad (10)$$

where $I_0(E_\gamma, s)$ is a dimensionless integration:

$$\begin{aligned} I_0(E_\gamma, s) &= \int_{E_\gamma + (m_\pi)^2/(4E_\gamma) - m_\pi}^{\infty} \frac{2d(E_\pi)}{p_\pi} \\ &\cdot \int_{E_p^{\text{threshold}}}^{\infty} d(E_p) \frac{\sigma_\pi(E_p)}{b(E_p)} \frac{dN(E_\pi, T_p)}{d(E_\pi)} \cdot n_{\text{gas}} v_p \frac{(p_p)^{1-s}}{s-1} \end{aligned} \quad (11)$$

Notice that the energy loss rate scales with gas density: $b \propto n_{\text{gas}}$ (see eqs. 9, A1, and A2). This exactly cancels the gas density in the numerator of eq. (11), and thus *the gamma-ray emission is independent of the gas density*. This is characteristic of calorimetry. Note further that the ratio b/n_{gas} depends only on the cross sections in the loss interactions. This means that I_0 and thus the gamma-ray emission depends only on the ratio of cross sections (inelastic pion production to total losses).

To account for the contribution from particle interactions involving nuclei with atomic weights $A > 1$ in both CRs and ISM, a nuclear enhancement factor of $\mathcal{A} = 0.59$ is included in the calculation. In the case of calorimetry, AppendixC shows that the ”nuclear enhancement” $\mathcal{A} = 1/\langle A \rangle$ and so $\mathcal{A} < 1$, this arises because additional nuclei species must share a fixed CR injection energy budget.

Let d to be the distance of the source, γ -ray flux can be expressed as:

$$E_\gamma^2 F_\gamma = E_\gamma^2 \frac{dN_\gamma}{dE_\gamma dAdt} = \mathcal{A} \frac{\epsilon_{\text{cr}} R_{\text{sn}}}{I(E_{\text{min}})} \cdot E_\gamma^2 \cdot \frac{1}{4\pi d^2} \cdot I_0(E_\gamma, s) \quad (12)$$

and the gamma-ray energy luminosity from the galaxy is:

$$L_\gamma = \frac{dE_\gamma}{dt} = \int E_\gamma \frac{dq_\gamma}{dE_\gamma} dE_\gamma dV = \mathcal{A} \frac{\epsilon_{\text{cr}} R_{\text{sn}}}{I(E_{\text{min}})} \cdot \int dE_\gamma E_\gamma \cdot I_0(E_\gamma, s) \quad (13)$$

Note that the volume integration in our one-zone model cancels the factor in the emissivity q_γ (eq. 10), leading to the final result that is independent of volume. We see therefore that in our calorimetric limit, the ratio L_γ/R_{SN} depends on the supernova acceleration parameters ϵ_{cr} and s , as well as I_0 which as we have noted depends only on cross sections. It is *independent* of gas density, volume, or mass.

The luminosity L_γ is proportional to R_{SN} , which usually is not measured, but is proportional to the star-formation rate of a galaxy. Therefore we can get

$$\frac{L_\gamma}{\psi} = \frac{0.00914 M_\odot^{-1} \mathcal{A} \epsilon_{\text{cr}}}{I(E_{\text{min}})} \cdot \int dE_\gamma E_\gamma \cdot I_0(E_\gamma, s) \quad (14)$$

which is a constant only depend on CR proton spectral index s in a calorimetric limit ($\epsilon_{\text{cr}} = 0.3\text{foe}$, with $1\text{foe} \equiv 10^{51}\text{erg} \equiv 1\text{Bethe}$). L_γ/ψ is observable, so it can be used to investigate cosmic-ray properties in a calorimetric system.

We can see that, our model's gamma-radiation results only depend on two parameters: cosmic-ray proton acceleration energy per supernova ϵ_{cr} (direct proportionality) and the proton injection spectral index s . We only need to vary the two parameters ϵ_{cr} and s to find the best fit to the model, which we will do below (§4.1).

3. Order-Of-Magnitude Estimates

An order of magnitude calculation of our model will help to give a sense of the final results and frame key physical issues. We aim to find the calorimetric gamma-ray emission from individual starburst galaxies.

For a starburst galaxy, the injected cosmic-ray energy rate got from supernovae exploration is:

$$\begin{aligned} dE_{\text{CR}}/dt &= f_{\text{cr}} E_{\text{SN}} \cdot R_{\text{SN}} = \epsilon_{\text{cr}} R_{\text{SN}} \\ &= \int E_{\text{p}} dN_{\text{p}}/dt = L_{\text{CR}} \end{aligned} \quad (15)$$

assuming the injected cosmic-ray spectrum is a power law in momentum here, $q_{\text{p}} = dN_{\text{p}}/dE_{\text{p}}dt = dq_{\text{p}}/dp_{\text{p}} = C p_{\text{p}}^{-s}$, $dE_{\text{CR}}/dt = C \int_{p_{\text{min}}} E_{\text{p}} p_{\text{p}}^{-s} dp_{\text{p}}$, $dN_{\text{CR}}/dt = C \int_{p_{\text{min}}} p_{\text{p}}^{-s} dp_{\text{p}}$, where C is a constant, p_{min} is the minimal momentum of injected CR protons which can be accelerated by SN.

Our model assumes all cosmic-rays will interact with interstellar medium, the interactions involve both elastic and inelastic scattering, in the GeV energy range. Thus we can get a crude estimation that the elastic scattering CR number is about the same as the inelastic number, i.e. $dN_{\text{CR,inelastic}}/dt \sim dN_{\text{CR,elastic}}/dt \sim (dN_{\text{CR}}/dt)/2$. For the inelastic scattering, only neutral pions could decay into photons, which take up one third of the total produced pion numbers, therefore $dN_\gamma/dt = 2dN_{\pi^0}/dt \sim 2(dN_{\text{CR,inelastic}}/dt(E_{\text{CR}} > E_{\text{threshold}}))/3 \sim (dN_{\text{CR}}/dt(E_{\text{CR}} >$

$E_{\text{threshold}})/3 = \dot{N}_{\text{CR,threshold}}$, where $E_{\text{threshold}}$ is the threshold kinetic energy of CR proton which can produce a pion.

$$\dot{N}_{\text{CR,threshold}} = dN_{\text{CR}}/dt(E_{\text{CR}} > E_{\text{threshold}}) \propto \int_{p_{\text{threshold}}} p_{\text{p}}^{-s} dp_{\text{p}} \propto \frac{p_{\text{threshold}}^{1-s}}{s-1} \quad (16)$$

In this case, we can get an estimation of the gamma-ray (number) flux from the thick-target model is:

$$\begin{aligned} F_{\gamma} &= \frac{1}{4\pi d^2} \frac{dN_{\gamma}}{dt} \\ &= \frac{1}{4\pi d^2} \cdot \frac{dN_{\gamma}/dt}{dE_{\text{CR}}/dt} \cdot dE_{\text{CR}}/dt \\ &= \frac{1}{4\pi d^2} \cdot \epsilon_{\text{cr}} \cdot R_{\text{SN}} \cdot \frac{1}{3} \cdot f_{\text{threshold}} \end{aligned} \quad (17)$$

where $f_{\text{threshold}} = \dot{N}_{\text{CR,threshold}}/L_{\text{CR}}$ is the average CR injected energy per above-threshold proton.

If $p_{\text{p}} < m_{\text{p}}$, protons can be approximated to be nonrelativistic, thus $E_{\text{p}} \approx p_{\text{p}}^2/2m_{\text{p}}$, while if $p_{\text{p}} > m_{\text{p}}$, protons can be approximated to be relativistic, $E_{\text{p}} \approx p_{\text{p}}$, and $2 < s < 3$, therefore we have:

$$\begin{aligned} L_{\text{CR}} &\propto \int_{p_{\text{min}}} E_{\text{p}} p_{\text{p}}^{-s} dp_{\text{p}} \\ &\propto \int_{p_{\text{min}}}^{m_{\text{p}}} \frac{p_{\text{p}}^2}{2m_{\text{p}}} p_{\text{p}}^{-s} dp_{\text{p}} + \int_{m_{\text{p}}}^{\infty} p_{\text{p}}^{1-s} dp_{\text{p}} \\ &\propto \frac{m_{\text{p}}^{2-s}}{2(3-s)} \left[1 + \frac{6-2s}{s-2} - \left(\frac{p_{\text{min}}}{m_{\text{p}}} \right)^{3-s} \right] \end{aligned} \quad (18)$$

For fixed s , $\delta L_{\text{CR}} \sim (\delta p_{\text{min}}/m_{\text{p}})^{3-s} \sim (\delta E_{\text{min}}/m_{\text{p}})^{\frac{3-s}{2}}$, when $s=2.2$, $\delta L_{\text{CR}} \sim (\delta E_{\text{min}}/m_{\text{p}})^{0.4}$. Therefore for $2 < s < 3$, we can see that L_{CR} from CR spectrum is insensitive to p_{min} , which is a good thing as there is no accurate determination of p_{min} , and most L_{CR} comes from $p_{\text{p}} \sim m_{\text{p}}$.

Let $s = 2.2$, $f_{\text{cr}} = 0.1$, $E_{\text{SN}} = 10^{51} \text{erg}$, $\epsilon_{\text{cr}} = 10^{50} \text{erg}$, $E_{\text{min}} = 0.001 \text{GeV}$, $E_{\text{threshold}} = 0.28 \text{GeV}$, the estimated gamma-ray flux for a certain starburst galaxy with the distance d and supernova rate R_{SN} is $F_{\gamma} \approx 3.31 \times 10^{50} R_{\text{SN}}/d^2$. For the starburst galaxy NGC253, our order of magnitude estimation gives the flux to be $4.57 \times 10^{-9} \text{cm}^{-2} \text{s}^{-1}$, agrees with *Fermi* measurement $10.7 \pm 2.1 \times 10^{-9} \text{cm}^{-2} \text{s}^{-1}$ (Hayashida et al. 2013) in an order of magnitude. Other starburst galaxies also have the similar agreements. The actual calculated results and detailed discussions see § 4.

4. Model Results

The thick-target model built in § 2 gives proportionality relation of the differential gamma-ray emission to ϵ_{cr} , and from eq 10, we can see that q_{γ}/L_{CR} is the same for every calorimetric galaxy

with the same choice of source CR proton index s , therefore

$$\frac{dL_\gamma/dE_\gamma}{L_{\text{CR}}} = \frac{\mathcal{A}E_\gamma dN_\gamma/dE_\gamma dt}{L_{\text{CR}}} \stackrel{\text{cal}}{=} E_\gamma \frac{I_0(E_\gamma, s)}{I(T_{\text{min}})} \text{GeV}^{-1} = \text{const} \quad (19)$$

and the relation is shown in Fig. 1 with $s = 2.2$ and 2.4 . Because $(dL_\gamma/dE_\gamma)/L_{\text{CR}}|_s$ is the same for calorimetric galaxy, the plot of this ratio presents the general properties of our model’s results: gamma-ray emission peaks around $\sim 0.15\text{GeV}$ and is nearly a power law at high energy. For different s , the ratios of differential gamma-ray luminosity to CR luminosity are different especially at high energy, but are always smaller than $1/3$ due to energy conservation.

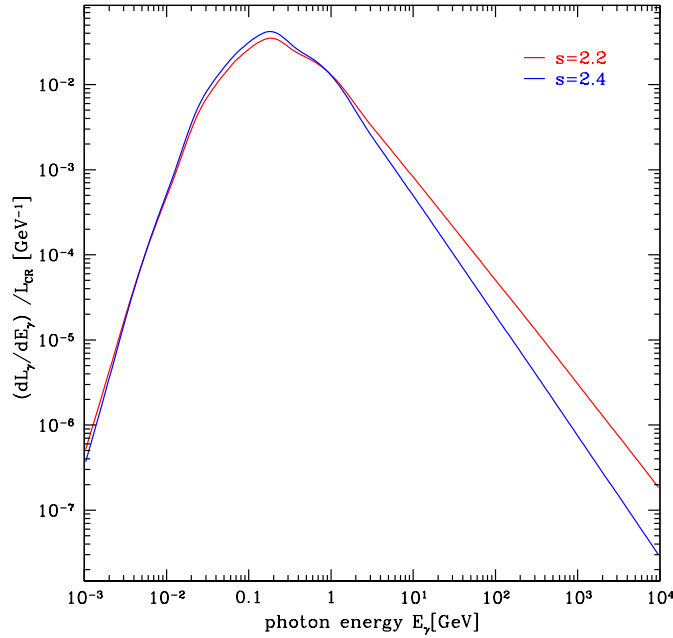


Fig. 1.— Ratio of differential gamma-ray luminosity to total CR luminosity for a calorimetric galaxy. The red line represents the result with choice of source CR index $s = 2.4$, while the blue line is for $s = 2.2$.

We now apply our model to individual starburst galaxies (§4.1). With their cosmic-ray parameters determined, we then compute their luminosity and evaluate their status as calorimeters (§4.3).

4.1. Individual Starbursts

We now apply our thick-target model to five individual starbursts NGC253, M82, NGC4945, NGC1068, and the Circinus galaxy, as well as the ULIRG Arp220. The input parameters and best-fit results are listed in Table 1 and Table 2. For each galaxy we adopt an observed star-formation

rate (SFR), and then calculate the pionic flux $E_\gamma^2 dN_{\pi \rightarrow \gamma\gamma} / dE_\gamma dAdt$ for each point in $(\epsilon_{\text{cr}}, s)$ space. We perform χ^2 test with the observed gamma-ray data to get the best-fit model parameters:

$$\chi^2(\epsilon_{\text{cr}}, s) = \sum_i \frac{(F_i - \hat{F}_i)^2}{\sigma_i^2} \quad (20)$$

where \hat{F}_i is the flux value of the data points at each photon energy E_i , $F_i = \epsilon_{\text{cr}} y_i(s)$ is our model's flux value at each E_i , σ_i is the uncertainty of the data's flux value at each E_i .

Table 1: Parameters set for the starburst galaxies in Thick-Target Model.

Galaxy Name	Distance D [Mpc]	SFR ψ [M_\odot/yr]	SN Rate R_{SN} [century $^{-1}$]	GeV data reference	TeV data reference
M82	3.4 ± 0.9	6.3 ± 0.9	5.7 ± 0.9	Ackermann et al. (2012)	Acciari et al. (2009)
NGC253	2.5 ± 0.5	2.9 ± 0.4	2.6 ± 0.4	Paglionie & Abrahams (2012)	Abramowski et al. (2012)
NGC4945	3.7 ± 0.8	3.5 ± 1.0	3.2 ± 0.9	Ackermann et al. (2012)	
NGC1068	16.7 ± 3.0	38 ± 10	35 ± 9	Ackermann et al. (2012)	Aharonian et al. (2005)
Circinus	4.2 ± 0.7	2.1 ± 0.5	1.9 ± 0.5	Hayashida et al. (2013)	
Arp220	77.0 ± 2.0	188.3 ± 10.0	172.1 ± 9.1	Peng et al. (2016)	Fleischhack et al (2015)

Galaxy distances: Gao & Solomon (2004). Star formation rates: Ackermann et al. (2012) using Gao & Solomon (2004) total IR luminosities and Kennicutt relation (Kennicutt 1998), except for the Circinus galaxy (Tully et al. 2009; Hayashida et al. 2013) and Arp220 (Peng et al. 2016).

Distance uncertainties come from <http://ned.ipac.caltech.edu>. Except for the ULIRG Arp220, the redshift-dependent distance uncertainty comes from Hubble constant error (Planck Collaboration et al. 2015) (assuming the peculiar velocity uncertainty is the same as Hubble constant uncertainty).

Table 2: Results for the starburst galaxies in Thick-Target Model.

Galaxy Name	CR source index \hat{s}	CR acceleration energy per SN ϵ_{cr} [foe/SN]	$L_{0.1-100\text{GeV}}^{\text{model}}$ [10^{40}ergs^{-1}]	$L_{0.1-100\text{GeV}}^{\text{Fermi}}$ [10^{40}ergs^{-1}]	Γ^{Fermi}
M82	2.275 ± 0.102	0.106 ± 0.025	1.48 ± 0.44	1.47 ± 0.14	2.25 ± 0.13
NGC253	2.350 ± 0.037	0.116 ± 0.013	0.73 ± 0.10	0.60 ± 0.07	2.18 ± 0.09
NGC4945	2.400 ± 0.446	$0.210(> 0.103)$	$1.64(> 0.80)$	1.17 ± 0.23	2.05 ± 0.13
NGC1068	2.100 ± 0.617	$0.253(> 0.128)$	$13.3(> 6.7)$	15.0 ± 2.9	2.29 ± 0.19
Circinus	2.300 ± 0.486	$0.619(> 0.310)$	$2.97(> 1.48)$	2.9 ± 0.5	2.19 ± 0.12
Arp220	2.550 ± 0.257	$0.808(> 0.404)$	$2.85(> 1.43) \times 10^2$	$(1.78 \pm 0.3) \times 10^2$	2.35 ± 0.16

Fermi gamma luminosities for the galaxies are calculated by Hayashida et al. (2013) using a power law spectral model $dN/dE \propto E^{-\Gamma}$, except for Arp220 Peng et al. (2016).

We consider injection indices in the range $s \in [2.1, 3.0]$. By maximizing the value of χ^2 at each s , we can get the best-fit values of ϵ_{cr} analytically. We then compare the values of χ^2 for each s with the best-fit ϵ_{cr} , finally can find the best-fit value of s numerically:

$$\frac{\partial \chi^2}{\partial \epsilon_{\text{cr}}} = 0 \Rightarrow \epsilon_{\text{cr, best-fit}} = \frac{\sum_i (y_i F_i / \sigma_i^2)}{\sum_i (y_i^2 / \sigma_i^2)} \quad (21)$$

The errors for the parameters s and ϵ_{cr} as well as gamma-ray flux F_γ can be obtained through likelihood function $P(\epsilon_{\text{cr}}, s)$:

$$\begin{aligned}
P(\epsilon_{\text{cr}}, s) &\propto \exp[-\chi^2(\epsilon_{\text{cr}}, s)/2] \\
\Rightarrow \sigma_{\epsilon_{\text{cr}}}^2 &= \frac{\sum_{2.1}^{3.0} ds \int_0^\infty d\epsilon_{\text{cr}} (f_{\text{cr}} - \epsilon_{\text{cr, best-fit}})^2 P(\epsilon_{\text{cr}}, s)}{\sum_{2.1}^{3.0} ds \int_0^\infty d\epsilon_{\text{cr}} P(\epsilon_{\text{cr}}, s)}, \\
\sigma_s^2 &= \frac{\sum_{2.1}^{3.0} ds \int_0^\infty d\epsilon_{\text{cr}} (s - s_{\text{best-fit}})^2 P(\epsilon_{\text{cr}}, s)}{\sum_{2.1}^{3.0} ds \int_0^\infty d\epsilon_{\text{cr}} P(\epsilon_{\text{cr}}, s)}, \\
\Rightarrow \sigma_{F_\gamma}^2 &\geq (dF_\gamma/d\epsilon_{\text{cr}})^2 \sigma_{\epsilon_{\text{cr}}}^2 + (dF_\gamma/ds)^2 \sigma_s^2
\end{aligned} \tag{22}$$

From Table 2, we can see that the pionic gamma-ray luminosity calculated from our model agrees well with the phenomenological *Fermi* fits for the starburst galaxies M82, NGC253, NGC4945, NGC1068 the Circinus galaxy, and ULIRG Arp220.

The best-fit pionic gamma-ray spectra can be seen in Figs. 2 through 5. In left panels, the solid lines is our model's calculated differential spectral energy distribution of the five starburst galaxies with the best-fit parameters s and ϵ_{cr} . The red points in GeV range are *Fermi* data while blue ones in TeV range are got from *H.E.S.S* or *VERITAS*. For M82 and NGC253, we see that our best fit to GeV and TeV data is quite good and fairly well constrained thanks to the relatively large energy range. For NGC1068, NGC4945, Circinus and Arp220, only GeV data is available and even our simple model is poorly constrained. In right panels, integrated spectral of the starburst galaxies are shown. Because *Fermi* actually measure the photon counts per certain energy range, the flux data points are calculated under power-law assumption of the spectral, it's more direct and reasonable to compare the value of integrated flux over certain energy range between our model and *Fermi* data. We can get pretty good fit to in each GeV energy range in the integrated spectral plots.

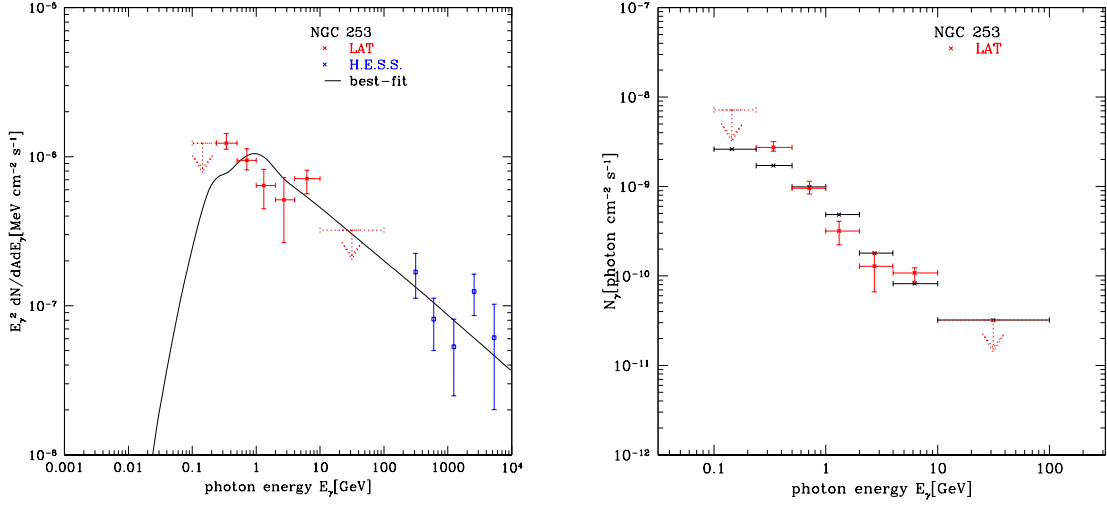


Fig. 2.— Left panel: Differential pionic gamma-ray spectrum (solid curve) for NGC253 with the best-fit parameters: source CR index s and accelerated CR energy per SN ϵ_{cr} . *Fermi* points are stars (red), *H.E.S.S.* points are squares (blue), black solid line is our model's best-fit to data; see Table 2. Right panel: Best-fit integrated pionic gamma-ray spectrum for NGC253. Red points are *Fermi* measurement, black points are our model's best-fit results.

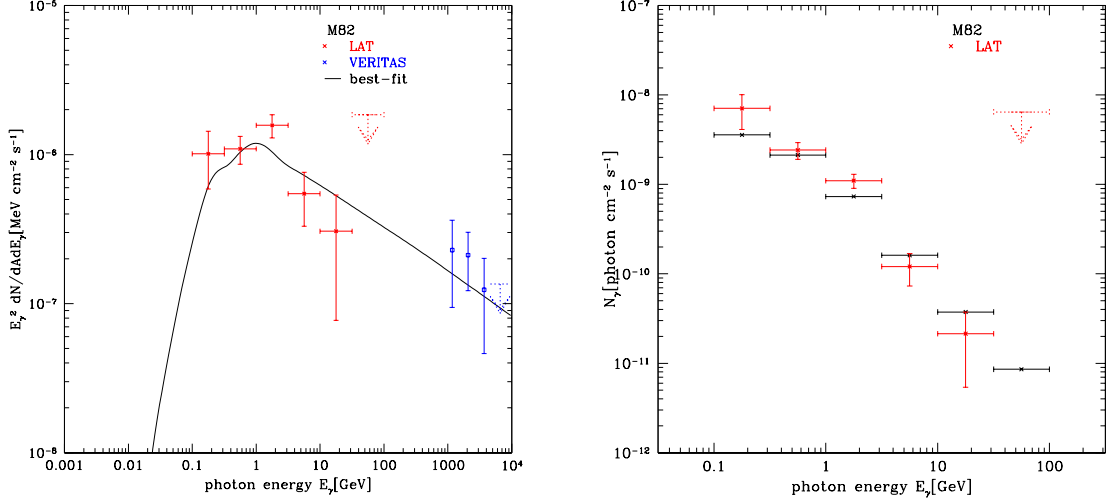


Fig. 3.— Left panel: Differential pionic gamma-ray spectrum (solid curve) for M82 with the best-fit parameters: source CR index s and accelerated CR energy per SN ϵ_{cr} . *Fermi* points are stars (red), *VERITAS* points are squares (blue), black solid line is our model's best-fit to data; see Table 2. Right panel: Best-fit integrated pionic gamma-ray spectrum for M82. Red points are *Fermi* measurement, black points are our model's best-fit results.

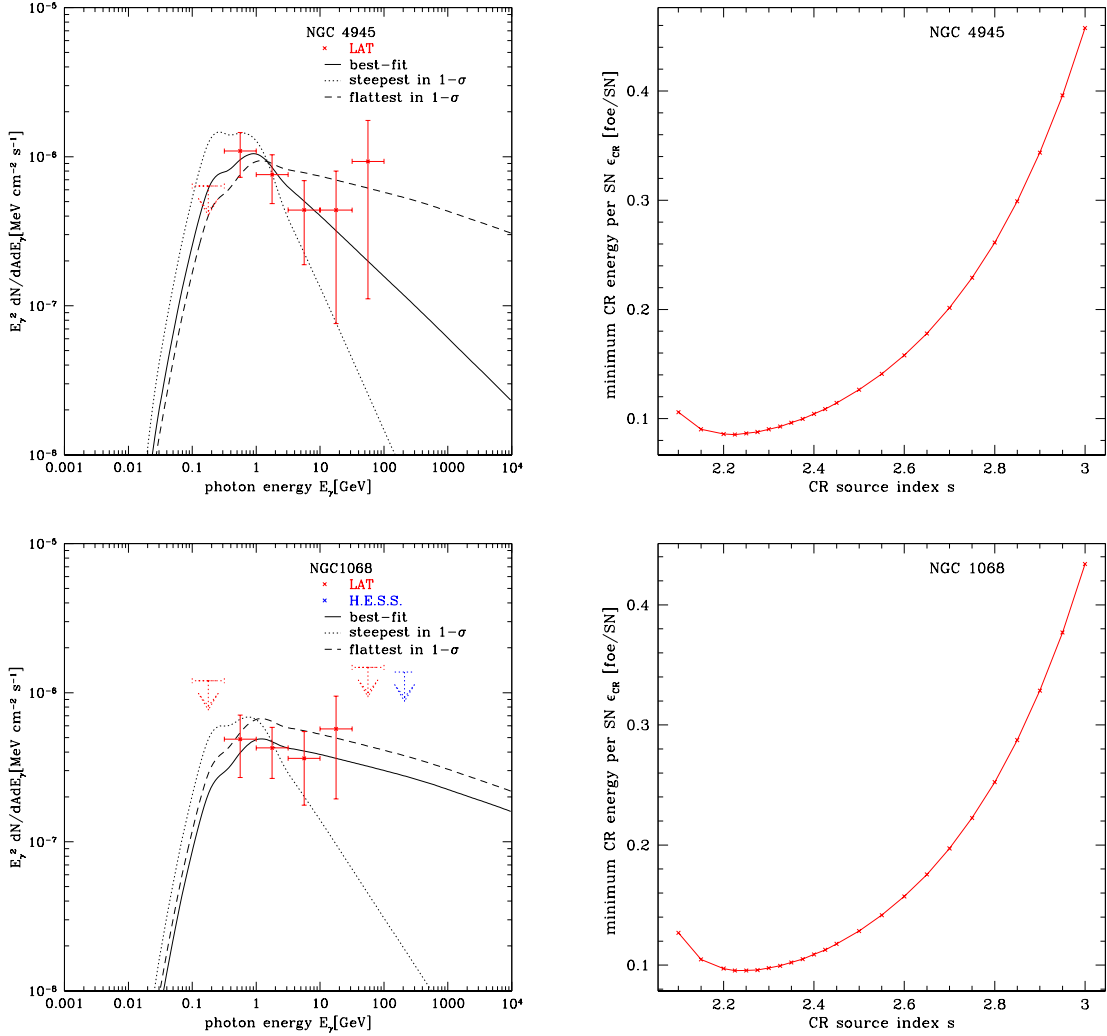


Fig. 4.— Left panel: Pionic gamma-ray spectra (solid curve) for NGC4945 (upper) and NGC1068 (lower) with the best-fit parameters: source CR index s and accelerated CR energy per SN ϵ_{CR} . *Fermi* points are stars (red), *H.E.S.S.* points are squares (blue), black solid line is our model’s best-fit to data; see Table 2. Black dashed line is our model’s flattest curve to fit the data in 1- σ error, while black dotted line is the steepest curve in 1- σ error, the parameters’ values of these curves are the cross points in Fig. 6. Right panel: minimum ϵ_{CR} vs. s for NGC4945 (upper), NGC1068 (lower).

From Figs. 2 through 5, we can see that the gamma-ray spectra got from our thick-target model has the following features, as already seen in Fig. 1: (1) the shape only depends on the injected proton spectrum; (2) the magnitude is proportional to ϵ_{CR} ; (3) at high energies, the gamma-ray spectral index is the same as the proton injection index s , and is flatter than in the escape-dominated galaxies (whether the gamma spectral index is same as the proton propagation index); (4) the peak position is insensitive to s , located at $E_\gamma \sim 1$ GeV where the two gamma-ray photons each get half of the rest-mass energy of the decayed π^0 , i.e., it has a “pion-bump” feature (Stecker

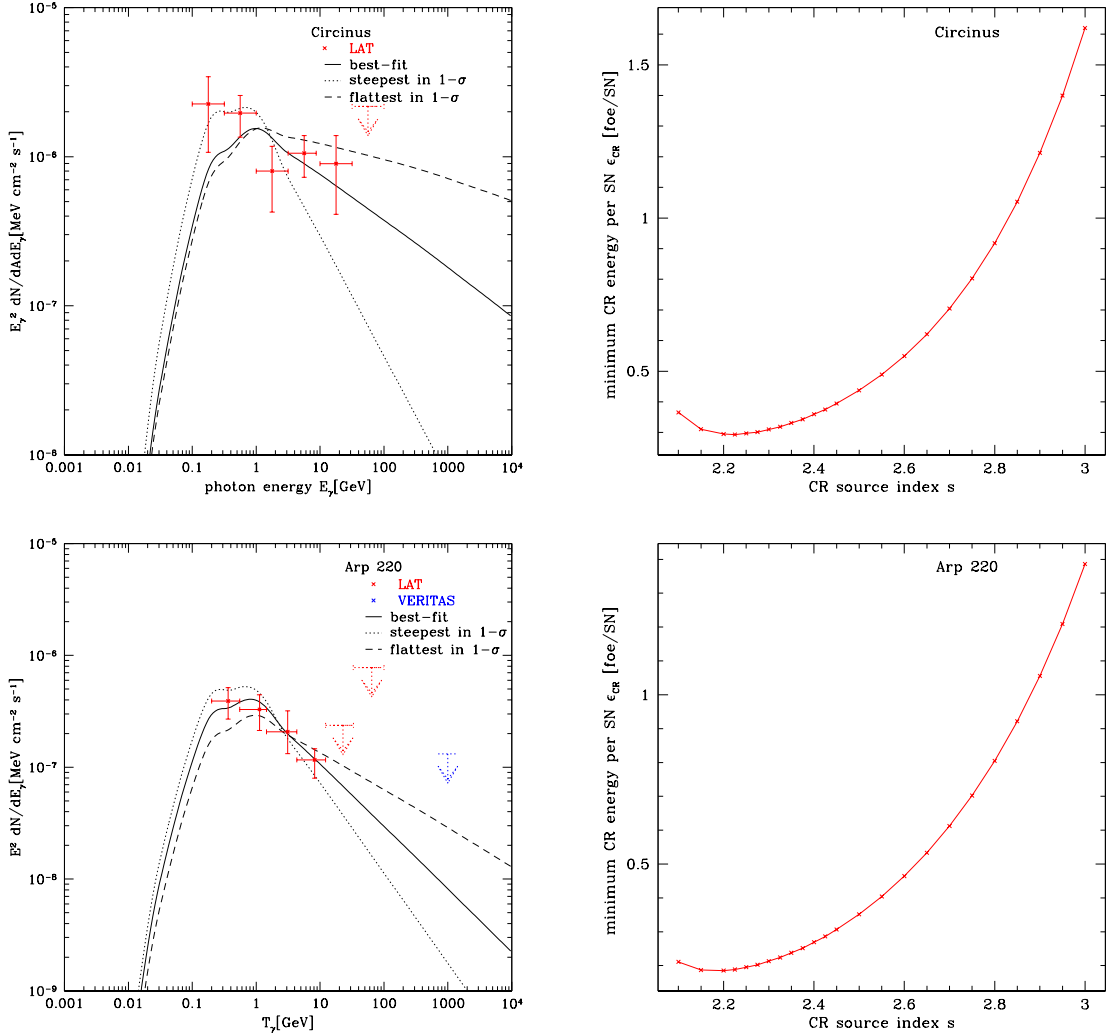


Fig. 5.— Left panel: Pionic gamma-ray spectra (solid curve) for the Circinus Galaxy (upper) and Arp220 (lower) with the best-fit parameters: source CR index s and accelerated CR energy per SN ϵ_{CR} . *Fermi* points are stars (red), *VERITAS* points are squares (blue), black solid line is our model’s best-fit to data; see Table 2. Black dashed line is our model’s flattest curve to fit the data in 1- σ error, while black dotted line is the steepest curve in 1- σ error, the parameters’ values of these curves are the cross points in Fig. 6. Right panel: minimum ϵ_{CR} vs. s for the Circinus Galaxy (upper) and Arp220 (lower).

1971; Dermer 1986).

The χ^2 contour plots are shown in Fig. 6 with CL= (70%, 95%, 99%). Both M82 and NGC253 have TeV data and good GeV data, and thus both s and ϵ_{CR} are well-constrained. For these galaxies, we find $\epsilon_{CR} \sim 0.1$ foe, in good agreement with canonical estimates for Milky Way cosmic rays (Ginzburg & Syrovatskii 1964). There is a positive correlation between s and ϵ_{CR} , i.e. in the same error range, the choice of larger s gives larger ϵ_{CR} . But for NGC1068, NGC4945, Circinus and

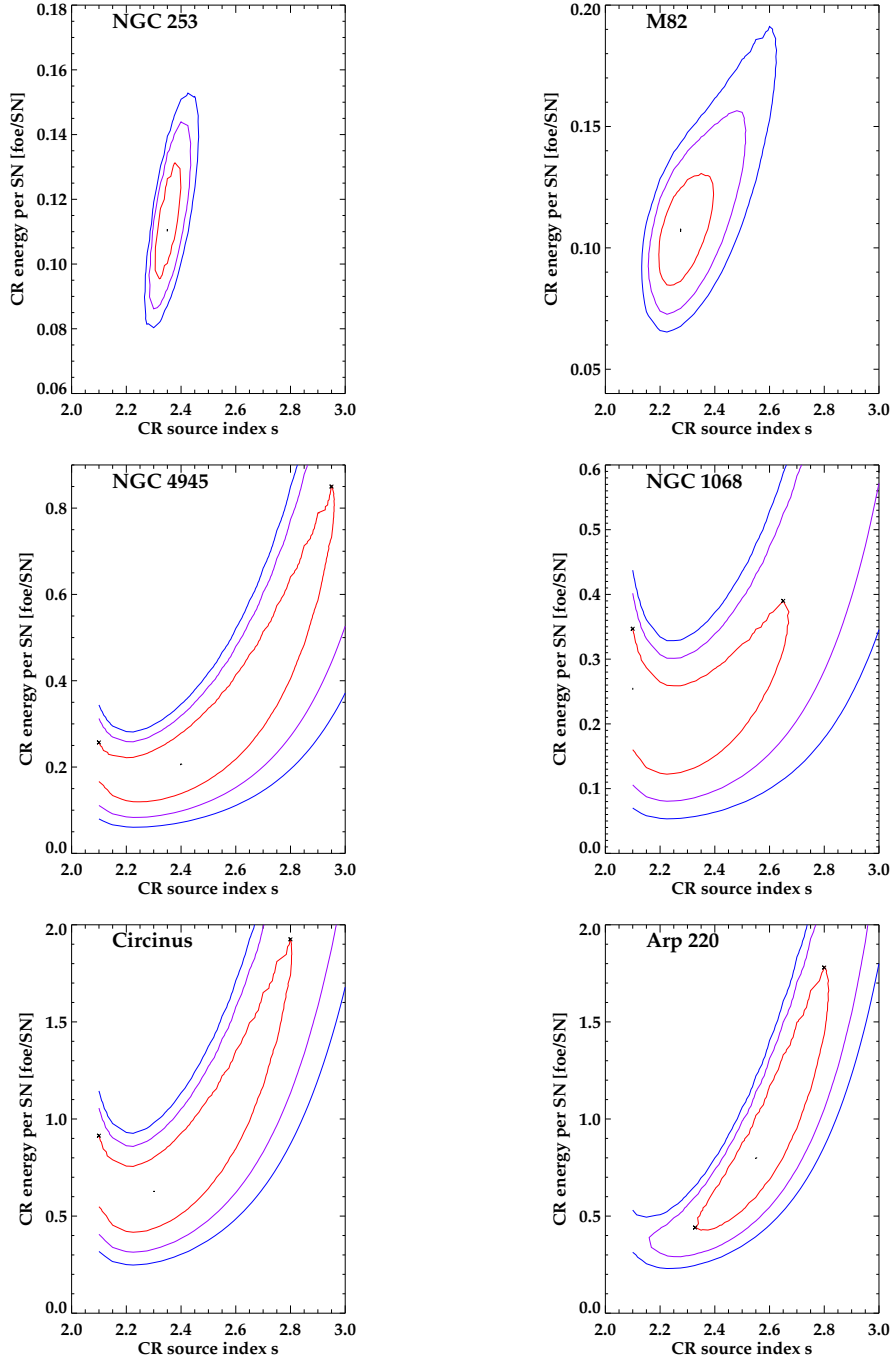


Fig. 6.— Contour plots of χ^2 for our model fits to starburst galaxy data. The best-fit values are the central black dot; (red, magenta, blue) lines represent (70% CL, 95% CL, 99% CL). For starbursts without TeV data and the ULIRG Arp220, the $1-\sigma$ fit values of the flattest and steepest curves are the cross points, the corresponding curves are shown in Fig. 4 and Fig. 5.

Arp220, lack of TeV data leaves the parameters poorly constrained, with large uncertainties in *both* s and ϵ_{cr} . In fact, the uncertainties are so large that it's more practical and reasonable to calculate the minimum value of ϵ_{cr} vs. s instead of calculating the errors:

$$P(> \epsilon_{\text{cr},\text{min}}) = \frac{\int_{\epsilon_{\text{cr},\text{min}}}^{\infty} d\epsilon_{\text{cr}} P(\epsilon_{\text{cr}}, s)}{\int_0^{\infty} d\epsilon_{\text{cr}} P(\epsilon_{\text{cr}}, s)} = 1 - \frac{\int_0^{\epsilon_{\text{cr},\text{min}}} d\epsilon_{\text{cr}} P(\epsilon_{\text{cr}}, s)}{\int_0^{\infty} d\epsilon_{\text{cr}} P(\epsilon_{\text{cr}}, s)} \quad (23)$$

Assume $y_i(s)$ is independent of ϵ_{cr} , $\hat{\sigma}^2 = 1/\sum_i y_i^2/(2\sigma_i^2)$, then

$$\begin{aligned} P(\epsilon_{\text{cr}}, s) &\propto \exp[-(\epsilon_{\text{cr}} - \epsilon_{\text{cr},\text{best-fit}})^2/\hat{\sigma}^2] \\ \Rightarrow \int_0^{f_{\text{cr}}} d\epsilon'_{\text{cr}} P(\epsilon'_{\text{cr}}, s) &\propto \hat{\sigma} \operatorname{erf}\left(\frac{\epsilon_{\text{cr}} - \epsilon_{\text{cr},\text{best-fit}}}{\hat{\sigma}}\right) \\ \Rightarrow P(> \epsilon_{\text{cr},\text{min}}) &= 1 - \operatorname{erf}\left(\frac{\epsilon_{\text{cr},\text{min}} - \epsilon_{\text{cr},\text{best-fit}}}{\hat{\sigma}}\right)/\operatorname{erf}(\infty) = 1 - \operatorname{erf}\left(\frac{\epsilon_{\text{cr},\text{min}} - \epsilon_{\text{cr},\text{best-fit}}}{\hat{\sigma}}\right) \end{aligned} \quad (24)$$

Let $P(> \epsilon_{\text{cr},\text{min}}) = 95\%$, we can get $\epsilon_{\text{cr},\text{min}}$ in 95% CL. The results are plotted in the left panels of Fig 4 and Fig 5, we can see that $\epsilon_{\text{cr},\text{min}}$ is sensitive to s , and blows up as s increases. Therefore TeV data is important for these starburst galaxies to constrain source CR spectral index s and thus getting better-constrained value for ϵ_{cr} .

For starbursts and Arp220 without TeV data, we also plot the flattest and steepest curves (the parameters values are the cross points in the contour plots Fig. 6) in addition to the best-fit curves (the parameters values are the central points in Fig. 6) to show a range of the curve distributions within $1 - \sigma$ error. The flattest curves are easier to be detected with larger TeV flux, while the steepest are more pessimistic. Comparing these curves at TeV range with the sensitivities of *VERITAS*, *H.E.S.S* and *CTA*, *VERITAS* and *H.E.S.S* could measure the TeV signals from NGC1068, NGC4945 and the Circinus galaxy, while *CTA* could perform well for all the five starbursts, and may be able to detect Arp220 in a long-term observation as Arp220's TeV flux is around the sensitivity of *CTA* in 50 hours (Hassan et al. 2015).

4.2. Projectile CR Proton Index And Supernova Acceleration Energy/Efficiency

The source CR proton index s and CR acceleration energy per SN are the only two parameters our model. These remain unfortunately poorly understood at a fundamental level, but are crucial probes of cosmic-ray acceleration physics. But Milky Way SNR gamma-ray data together with supernova acceleration theories can give both observational and theoretical insight into the parameters we have derived for starbursts in the previous section.

Diffusive shock acceleration (DSA) is a prevailing acceleration mechanism for supernova remnant (SNR). DSA naturally yields a relativistic electron and ion spectra that are each power laws in momentum, in the test-particle limit that neglects feedback from the accelerated cosmic rays onto the shock (e.g., Krymskii 1977; Bell 1978; Blandford & Ostriker 1978). However, as many

others have found, and we will confirm, a substantial fraction of the shock energy is transferred to CR protons, with estimates in the Milky Way of a few to tens of percent (e.g., Fields et al. 2001; Lemoine-Goumard et al. 2012). Although the resulting non-linear correction to DSA results in a concave proton spectrum with a steeper spectrum index at high energy (e.g., Morlino & Blasi 2015; Kang et al. 2013; Slane et al. 2014), the concavity is expected to be rather mild for a SN with particle acceleration efficiency to be at the order of $\sim 10\%$ (Morlino & Blasi 2015). Thus for the simple model built in this paper, it is reasonable to assume a power-law distribution of accelerated CR.

For a strong shock in monatomic gas, DSA gives accelerated proton index $s \sim 2.0$. In GeV and TeV energy range, the combination of observed CR flux at Earth ($\propto E^{-2.75}$) and galactic CR transportation models (e.g., Strong & Moskalenko 1998; Evoli et al. 2008; Blasi & Amato 2012) implies the index s to be $2.2 - 2.4$ (Caprioli 2012). Other theories give different values of the source proton index value in SNR, for example, Dermer et al. (2013) gives 2.5 below 6.5 GeV and 2.8 above, for the interstellar cosmic-ray proton index; Lemoine-Goumard et al. (2012) get the proton spectral index is 1.8 for SNR RCW86; Morlino & Caprioli (2012)’s model for Tycho is 2.2. Gamma-ray emission from SNRs probes s directly (if pions dominate), and available measurements give s spanning a considerable range. *Fermi* LAT measurement of Galactic SNRs give $s = 1.53$ to 3.58 with the weighted average to be 2.39, while the spread of the index is about 1 (Acero et al. 2015). Because some SNRs are dominated by IC or bremsstrahlung which contribute to flatter photon spectra than pions, the actual source proton index estimated from *Fermi* SNR measurements would be steeper than the weighted average value of s . Particularly for the SNRs W44 and IC443 with clear characteristic pion-decay gamma-spectra, the observations give the accelerated proton index s to be about 2.4 in the energy range smaller than break energy (Ackermann et al. 2013), where the projectile CRs in the galaxies mainly come from. Moreover, for TeV gamma-rays, we expect the signal is pionic and thus these index measurements can give us a fair estimate of the CR source index. The TeV data gives the index varies between 1.8-3.1 with an average value $s \sim 2.4$ (e.g., Aliu et al. 2013; Brun et al. 2011; Aharonian et al. 2008). Therefore the values of source spectral index s obtained from our model for individual starbursts (~ 2.3) are reasonable.

For CR acceleration energy parameter, $\epsilon_{\text{cr}} = E_{\text{sn}} f_{\text{cr}}$, the average kinetic energy released per SN (E_{sn}) is 10^{51} erg (Woosley & Weaver 1995), but there exists much uncertainties in the value of SNR acceleration efficiency to CR (ϵ_{sn}). If SNRs are the main sites of acceleration of cosmic rays, then 3 to 30% of the supernova kinetic energy must end up transferred to CR protons from various theories: Fields et al. (2001) suggested that if SNRs are the dominate sources for cosmic-ray production as well as the nucleosynthesis of lithium, beryllium, and boron in the Milky Way, an acceleration efficiency of $\sim 30\%$ is needed; Strong et al. (2010) obtains a CR energy input efficiency per SN of $3 - 10\%$; Caprioli (2012)’s study also found the acceleration efficiency saturates at around $10 - 30\%$; Dermer & Powale (2013)’s results suggest that most supernova remnants accelerate cosmic rays with an efficiency of $\sim 10\%$ for the dissipation of kinetic energy into nonthermal cosmic rays. The observations of SNRs also give insight into CR acceleration efficiency, for example, SNR Tycho

accelerates protons up to 500 TeV with an efficiency of $\sim 10\%$ (Morlino & Caprioli 2012) while the hadronic scenario of SNR RCW86 concludes that the accelerated particles energy efficiency from SNR is at the level of ~ 0.07 (Lemoine-Goumard et al. 2012). Thus the initial value of $\epsilon_{\text{cr}} = 10\% \cdot 10^{51} \text{erg} = 0.1$ foe set in our model and the maximum value $\epsilon_{\text{cr,max}} = 0.3$ foe used as the calorimeter limit are feasible both theoretically and observationally.

4.3. Calorimetric Limit

From eq 14, we can see that the ratio of L_γ/ψ is a constant depending on s , because star formation rate ψ is related with total IR luminosity by Kennicutt (1998),

$$\frac{\psi}{M_\odot \text{yr}^{-1}} = \epsilon_{1.7} \times 10^{-10} \frac{L_{8-100\mu\text{m}}}{L_\odot} \quad (25)$$

$\epsilon_{1.7}=0.79$ is used here (Ackermann et al. 2012) for a Chabrier (2003) initial mass function (IMF). the ratio L_γ/L_{IR} is also a constant only depends on s :

$$\begin{aligned} L_\gamma/L_{8-100\mu\text{m}} &= \frac{\epsilon_{\text{cr}} 0.00914 M_\odot^{-1} \epsilon_{1.7} \times 10^{-10} M_\odot \text{yr}^{-1}}{L_\odot I(E_{\text{min}})} \cdot \mathcal{A} \int dE_\gamma E_\gamma \cdot I_0(E_\gamma, s) \\ &= \frac{0.003033}{I(E_{\text{min}})} \cdot \mathcal{A} \int dE_\gamma E_\gamma \cdot I_0(s) \end{aligned} \quad (26)$$

The expected calorimetric limit ratio $L_{>1\text{GeV}}/L_{8-100\mu\text{m}}$ for CR nuclei with $s = 2.0$ is 5.2×10^{-4} for our thick-target model, Lacki et al. (2011) calculated the ratio to be 3.1×10^{-4} while *Fermi* group's result is 2.5×10^{-4} (Ackermann et al. 2012), an agreement within an order of magnitude.

The systematic uncertainties of our calorimetric model's gamma-ray luminosity mainly come from two sources. One is the uncertainty in the L_{IR} -SN rate conversion. While the L_{IR} -SFR conversion introduces the error with a factor of 2-3 (Kennicutt 1998), the fact that both SN rate and far-IR luminosity arise from massive stars brings a cancellation of the error, making the final L_{IR} -SN rate calibration uncertainty as good as 10-20% (Horiuchi et al. 2011). The other main uncertainty in our model is the cross section σ_{pp} of $p-p$ reaction which is generally better than 10% (Olive & Particle Data Group 2014). Furthermore, the calorimetric gamma-ray luminosity derives from the ratio $\sigma_{\text{pp,inelastic}}/b(\sigma_{\text{pp,total}})$, making additional cancellation of the uncertainty. So the resultant calorimetric gamma-ray luminosity should be good to $\lesssim 30\%$ or better.

The gamma-ray luminosity over total IR luminosity ratio expected in the calorimetric limit for CR nuclei $L_{0.1-100\text{GeV}}/L_{8-100\mu\text{m}}$ is plotted in Fig 7 for different choices of CR proton index s . Note that our calorimetric limits agree with *Fermi* group's (Ackermann et al. 2012) within 30%, which is consistent within uncertainties.

In each of our calculations and plots for individual galaxies, the cosmic-ray acceleration efficiencies correspond to a mean value for all supernovae in the galaxy. We can compare this to typical

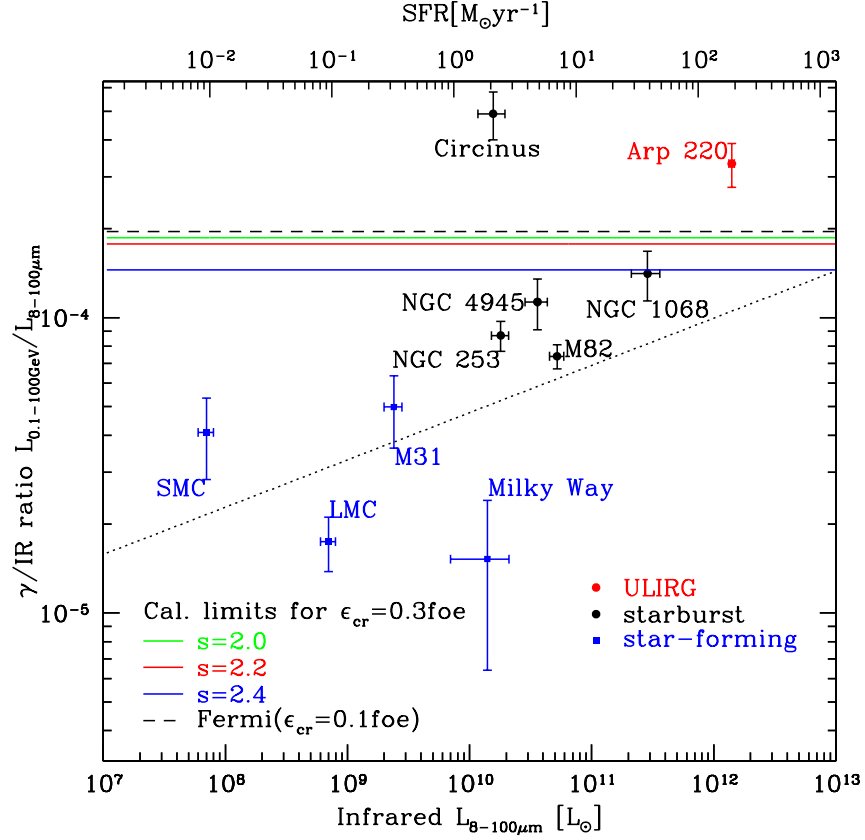


Fig. 7.— Plot of ratio of gamma-ray luminosity (0.1 – 100GeV) to total IR luminosity (8-100 μ m). Blue squares: ordinary star-forming galaxies; black points: starbursts; red: ULIRGs. Milky Way IR and gamma-ray from Strong et al. (2010), IR data for other galaxies from Sanders et al. (2003), gamma-ray data for SMC (Abdo et al. 2010), LMC (Abdo et al. 2010), M31 (Abdo et al. 2010)). Starburst IR data from Gao & Solomon (2004), gamma-ray data from Ackermann et al. (2012), except for the Circinus (Hayashida et al. 2013)) and Arp220 (Peng et al. 2016). The black dotted line: *Fermi*’s best-fit power law relation (Ackermann et al. 2012). Upper abscissa: SFR estimated from the IR luminosity (Kennicutt 1998). The blue solid line: calorimetric gamma-ray luminosity limit assuming an average CR acceleration energy per supernova of $\epsilon_{\text{cr}} = 3 \times 10^{50} \text{erg} = 0.3 \text{ foe}$ with source CR index $s = 2.4$; purple and green lines for $s = 2.2$ and $s = 2.0$ respectively. The black dashed line indicated *Fermi*’s calorimetric results ($s = 2.2$, $\epsilon_{\text{cr}} = 10^{50} \text{erg}$ (Ackermann et al. 2012)).

values of ϵ_{cr} for Milky Way supernovae taken from the literature. These values typically vary (e.g., Fields et al. 2001) from 0.1 foe to 0.3 foe. Detailed discussions see § 4.2. We provisionally adopt a *maximum* value of

$$\epsilon_{\text{cr,max}} = 0.3 \text{ foe} \quad (27)$$

in order to judge the proton calorimetry of the starbursts: if $\epsilon_{\text{cr}} > \epsilon_{\text{cr,max}}$, calorimetry fails for that galaxy, because our model gives an upper-limit to the gamma-ray spectrum, other dominant

gamma-ray sources must exist in that galaxy (e.g., AGNs), or the electron processes (inverse Compton and bremsstrahlung) dominate the gamma-ray emission from that galaxy with a much larger electron/proton ratio, to explain the gamma-ray signal; if $\epsilon_{\text{cr}} < \epsilon_{\text{cr,max}}$, the starburst is a proton calorimeter with the calorimetric efficiency to be $\epsilon_{\text{cr}}/\epsilon_{\text{cr,max}}$, i.e., M82 has a calorimetric efficiency of 35%, NGC253 is 39%, NGC1068 is 84% and NGC4945 is 70%. For the Circinus galaxy and the ULIRG Arp220, there are two possibilities: (1) the calorimetry relation fails and there exist other gamma-ray sources or the electron gamma-ray emission dominates; (2) the galaxy is a fully proton calorimeter (the calorimetric efficiency is 100%), but supernovae are substantially more efficient accelerators in the system, or supernova rates are underestimated by their far-infrared luminosities.

The proton calorimetry of the starbursts could also be judged by Fig. 7, which shows both the calorimetric limit from our model and but data for all star-forming galaxies with gamma-ray detections. Here we include two measurements of the ULIRG Arp 200. Griffin et al. (2016) measure the luminosity of Arp220 to be $8.22 \pm 3.0 \times 10^{41}$ ergs/s in the energy band $[0.8, 100]$ GeV, while our model’s calorimetric limit L_γ in the same energy range is 5.7×10^{41} ergs/s; another independent group Peng et al. (2016) report their gamma-ray luminosity to be $1.39 \pm 0.31 \times 10^{42}$ ergs/s in the energy band $[0.2, 100]$ GeV, while our calorimetric limit result is 0.95×10^{42} ergs/s. Therefore, although Arp220 is high above the calorimetric limits in Fig 7, within the errors, the observed gamma-ray luminosity is not far from or even compatible with our model’s calorimetric limit in the same energy range.

Fig. 7 allows us to draw several conclusions.

1. Normal, Milky-Way-like (“quiescent”) star-forming galaxies are about an order of magnitude below the calorimetric limits. This is as expected: Milky-Way Galactic cosmic rays are known to be escape-dominated and thus their cosmic rays find themselves in the thin-target regime, rather than thick-target calorimetric limit. We see that most ($\sim 90\%$) cosmic rays escape before interacting.
2. The starburst galaxies M82, NGC253, NGC1068 and NGC4945 are close to the limits, which shows that calorimetry is a good approximation for these galaxies. This further implies that quiescent and starburst galaxies occupy opposite limits of gamma-ray production.
3. Two galaxies lie above the calorimetric bounds. The Circinus galaxy lies substantially above these limits. For Arp220, the situation is somewhat less clear.

In the case that a galaxy’s gamma-ray emission truly exceeds our bound on proton calorimetry, there are several possible explanations. Two possibilities envision increased pionic emission from cosmic-ray protons. This could occur if a galaxy harbors supernovae that are systematically more efficient accelerators than in the present Milky Way, i.e., they exceed our adopted value $\epsilon_{\text{cr,max}} = 0.3$ foe (eq. 27). Presumably this would reflect systematically more energetic explosions and/or more favorable particle injection. A test for this scenario would be that cosmic-ray electron signatures should be similarly enhanced, e.g., radio synchrotron, or IC emission below the pion bump. A

higher pionic flux would also follow if supernova rates are underestimated by far-infrared luminosity measurements. This would require that *less* UV from massive stars is reprocessed by dust than in typical galaxies, which seems difficult to arrange in starburst and/or ULIRGs.

It of course is also possible that a galaxy exceeds the calorimetric bound because the gamma-ray emission is dominated by sources other than protons. Electron gamma emission could dominate if there is a much larger electron/proton ratio in the galaxy’s cosmic rays; this would imply that the gamma-ray flux should not show a pion feature. And finally, a galaxy can exceed our bound if it harbors an active nucleus in which a supermassive black hole jet powers gamma-ray emission. A signature here would be the time variability that is characteristic of most gamma-ray signals from active galaxies.

4.4. Neutrino estimation for individual starbursts

High energy accelerated CR protons also generate cosmic neutrinos in addition to gamma-ray photons, through the interaction between CRs and ISM (pp collisions) where both neutral and charged pions are created (e.g., Halzen & Hooper 2002). The charged pions decay to neutrinos via $\pi^+ \rightarrow \nu_\mu \bar{\nu}_\mu \nu_e e^+$ and $\pi^- \rightarrow \bar{\nu}_\mu \nu_\mu \bar{\nu}_e e^-$. Thus starburst galaxies are plausible high-energy neutrino source candidates (e.g., Loeb & Waxman 2006; Lacki et al. 2011) whose gamma-rays are accompanied by high-energy neutrinos.

In pp collisions, isospin considerations demand that $N_{\pi^\pm} \simeq 2N_{\pi^0}$ and the flavor ratio after oscillations is $\nu_e : \nu_\mu : \nu_\tau = 1 : 1 : 1$ for both neutrinos and antineutrinos (Kamae et al. 2006; Kelner et al. 2006). The differential fluxes of gamma-rays and single-flavor neutrino ($\nu_i + \bar{\nu}_i, i = e, \mu, \tau$) are related as $dF_{\nu_i}/dE_{\nu_i}(E_{\nu_i} = E_\gamma/2) = 2dF_\gamma/dE_\gamma(E_\gamma)$ ignoring absorption effects (Anchordoqui et al. 2004; Ahlers & Murase 2013; Murase et al. 2013). Therefore for a given starburst galaxy, we estimate the upper-limit to its neutrino flux at high energy by our model’s calorimetric pionic gamma-ray result and thus constrain the flux measured from neutrino telescopes like IceCube.

For the case of M82, our model gives a flux $F_{\gamma, 2\text{TeV}-2\text{PeV}} \sim 5.154 \times 10^{-14} \text{phcm}^{-2}\text{s}^{-1}$, the associated single-flavor neutrino flux (1TeV – 1PeV) would thus be $F_{\nu, 1\text{TeV}-1\text{PeV}} \sim 1.031 \times 10^{-13} \text{cm}^{-2}\text{s}^{-1}$, $dF_\nu/dE_\nu \sim 6.572 \times 10^{-14} (E_\nu/\text{TeV})^{-2.275} \text{cm}^{-2}\text{s}^{-1}$, $dF_\nu/dE_\nu(E_\nu = 1\text{TeV}) \sim 6.572 \times 10^{-14} \text{cm}^{-2}\text{s}^{-1}$. For IceCube, the median sensitivity at 90% C.L. is $\sim 10^{-12} \text{TeV}^{-1}\text{cm}^{-2}\text{s}^{-1}$ for energies between 1TeV – 1PeV with an E^{-2} spectrum and the upper-limit of M82 got by IceCube $\Phi_{\nu_\mu + \bar{\nu}_\mu}^{90\%} = 2.94 \times 10^{-12} \text{TeV}^{-1}\text{cm}^{-2}\text{s}^{-1}$ (IceCube Collaboration et al. 2014). Therefore our model’s estimated neutrino flux of M82 is well below the upper limit, and is more than 10 times too faint to be observed, in agreement with Lacki & Thompson (2013)’s conclusion. However, stacking searches of starbursts may get a detectable signal (Lacki et al. 2011) and the starbursts can contribute to the diffuse neutrino background which may be detectable by IceCube (Loeb & Waxman 2006).

5. Discussion and Conclusions

In this paper, we construct a two-parameter, closed-box, thick-target model to explain the gamma-ray emissions and test the cosmic-ray calorimetry of starburst galaxies.

Pohl (1993, 1994) presented a prescient theoretical study of the calorimetric behavior of galaxies in the EGRET era. He characterized star-forming galaxies in the thick-target limit as “fractional calorimeters” for both hadrons and leptons. Specifically, Pohl pointed out that fraction of cosmic-ray energy returned in gamma-rays reflects a combination of the fraction of particle loss mechanism which can lead to gammas, and the branching to gammas in those interactions. Our approach is guided by this point of view, and we now have the benefit of GeV and TeV data on starforming galaxies to test these ideas.

In addition, gamma-ray emission from starburst galaxies has been calculated by a number of groups (e.g., Paglione et al. 1996; Torres 2004; Persic et al. 2008; de Cea del Pozo et al. 2009; Lacki et al. 2010, 2011; Yoast-Hull et al. 2013; Eichmann & Becker Tjus 2016). These important papers follow calculation procedures similar to ours, and also solve the one-zone diffusion-loss equation (e.g., Meneguzzi et al. 1971; Longair 1981) to obtain steady-state particle spectrum and in turn the gamma-ray emission. However, these papers and ours differ in several assumptions, variables and formula numerical calculations. (1) Previous treatments use the general solution to the diffusion-loss equation with different parameter choices, except for (Yoast-Hull et al. 2013, 2014, 2015) which adopt an approximate solution with loss dominant assumption, while ours is a thick target approximation with a “closed-box” calculation which is much simpler to compute. (2) In order to get the pionic gamma-ray spectrum dq_γ/dE_γ (eq 8), we carry a full numerical integration subroutine of to get dq_π/dE_π (eq 7), while other groups either adopt the parameterization equations of differential cross section $d\sigma_\pi(E_p, E_\pi)/dE_\pi$ directly (e.g., Torres 2004; Domingo-Santamaría & Torres 2005) or use GALPROP code to calculate the differential cross section from pp collision (e.g., Lacki et al. 2010) or assume a delta function approximation for pion distribution (Yoast-Hull et al. 2013, 2014, 2015) or directly use the analytical form of the gamma energy distribution given by Kelner et al. (2006) (Eichmann & Becker Tjus 2016). (3) These calculations to various extents present multi-frequency and multi-process models, i.e., radio plus gamma-ray emission, with both leptonic process (synchrotron, bremsstrahlung and inverse Compton) and hadronic process (pion decay) in a more complex and realistic way. This naturally entails more free parameters like the source CR parameters for both electrons and protons, diffusion loss time scale, advection loss timescale, magnetic field, gas density.

Our model *by construction* is less ambitious than these other studies, but very well-defined. It is also particularly free of astrophysical uncertainties, because we only focus on thick-target pionic emission that requires only two parameters (s, ϵ_{cr}). Our results are, for example, independent of the galaxy’s gas density. Thus our model is targeted to (1) offer a particularly direct and simple means of estimating these fundamental parameters in starburst galaxies, thus measuring their cosmic-ray acceleration properties that can be compared with those in the Milky Way; and (2) place a firm

and careful upper limit to the hadronic gamma-ray luminosity of *any* star-forming galaxy.

For individual starburst galaxies, our model gives good fits to the gamma-ray data in both GeV and TeV range with proper choices of the injected proton index s and cosmic-ray proton acceleration energy per supernova ϵ_{cr} , showing the thick-target assumption is a plausible explanation of the observed starburst GeV and TeV emission. Our model shows that the gamma-ray spectrum of thick-target systems shares the same index as the CR “injection” index, instead of the CR propagated index. This contrasts with the “thin-target” situation that should correspond to ordinary star-forming galaxies like Milky Way. Our fit gives the average value of s in starbursts to be ~ 2.3 , which is consistent with the LAT measurement of Galactic SNRs with an average value of s to be 2.39 (Acero et al. 2015), implying that cosmic-ray acceleration by supernovae is broadly similar in starburst galaxies and the Milky Way.

The goodness of our fit of starbursts M82, NGC253, NGC1068 and NGC4945 suggest that starburst galaxies are proton calorimeters with calorimetric efficiencies vary from 35% to 84%. These efficiencies may be different in reality if the actual supernova acceleration of CR rate in starbursts differ from the maximum CR acceleration energy $\epsilon_{\text{cr,max}} = 0.3$ foe we have adopted (eq. 27); the scaling is simply $\epsilon_{\text{cr}}/\epsilon_{\text{cr,max}}$. For the Circinus galaxy, our model’s gamma-ray luminosity agrees with Hayashida et al. (2013), and is above our limit, as is the ULIRG Arp220. These excesses may be explained in two ways: (1) additional gamma-ray sources are needed to explain the observed data, or the electron processes dominate the gamma-ray production in the galaxy (e.g., Downes & Eckart 2007; Sakamoto et al. 2008; Wilson et al. 2014; Tunnard et al. 2015); (2) the galaxy is a fully proton calorimeter (Torres 2004; Lacki & Thompson 2013; Yoast-Hull et al. 2015), but supernovae are substantially more efficient accelerators in this system, or the supernova rates are underestimated by their far-infrared luminosities, i.e, the scaling relation between the far-infrared luminosity and star formation rate is different (e.g. Fox & Casper 2015).

Therefore we conclude that at least for currently observed starbursts, most are nearly or fully proton calorimeters. Others have addressed the question of proton calorimetry in starbursts. For example, Yoast-Hull et al. (2013, 2014) find M82 and NGC253 50% proton calorimeters, Ackermann et al. (2012) get calorimetric efficiencies of 30% – 50% for starburst galaxies with SFR $\sim 10\text{M}_{\odot}\text{yr}^{-1}$, while Lacki et al. (2010, 2011) conclude that proton calorimetry holds for starburst galaxies with $\Sigma_{\text{gas}} > 1\text{g cm}^{-2}$ and the calorimetric fraction is 0.2 for NGC253 and 0.4 for M82. Moreover, Torres (2004), Lacki & Thompson (2013) and Yoast-Hull et al. (2015) conclude that Arp220 is a hadronic calorimeter or nearly so. Our conclusions are consistent with these.

More data can further test starburst proton calorimetry. There are no published starburst data at energies $\sim 30\text{--}100$ MeV; observations in this regime should reveal the characteristic “pion bump.” TeV data for NGC1068, NGC4945, Circinus, and Arp220 is also needed to constrain the choices of parameters (both s and ϵ_{cr}) in our model with smaller uncertainty. If Arp 220 indeed saturates the proton calorimeter limit, it is the best example of a star-forming galaxy as a proton calorimeter, but it lies at the edge of GeV detectability and has no TeV measurements. As discussed in §4.1,

VERITAS or *H.E.S.S.* could measure the TeV signals from the starbursts NGC1068, NGC4945 and the Circinus galaxy within their sensitivities. Future *CTA* observations should dramatically improve our understanding of starburst galaxies, and may be able to detect Arp220 in a long-term dedicated observation.

The thick-target model presented here neglects primary electron effects (bremsstrahlung radiation, inverse Compton) and secondary electron effects in gamma-ray emission. This assumption is consistent with recent *NuSTAR* observation, the X-ray limits on NGC253 in the 7-20 keV band disfavors leptonic processes dominating in the GeV and TeV energy range (Wik et al. 2014). By assuming the CR protons lose energy continuously through the propagation inside the starbursts, the effect of secondary recoil protons (the ISM protons after pp collisions) appears only via the elastic scattering energy loss term, and not as a proton source term. While these effects should not dominate, they would only boost the gamma-ray production and lead to an even tighter limit to the gamma-ray emission. We also ignore the effect of intergalactic absorption of the high-energy gamma rays via photon-pair production ($\gamma\gamma \rightarrow e^+e^-$) in collision with background starlight emission (e.g., Salamon & Stecker 1998; Stecker et al. 2012), which will bring a steepening of the gamma-ray spectrum at high energy, but this effect is very small for the starbursts we study, which are all very nearby.

There still remains space to improve our model. Future work would benefit from better observational determination of galaxy distances, SFR rate or better SN rates, and of course well-measured TeV gamma-ray data. The particle experimental data adopted in our model is as old as from 1980s, we would like to call for new measurements of the $p-p$ reaction and the pion momentum distribution. These data are important not only for gamma-ray emissions but also for the inelastic losses of CRs. Theoretical work would benefit from additional multi-wavelength constraints on the cosmic-ray electrons (add leptonic process in our model). Finally, if a starburst could be resolved spatially, perhaps in the TeV, this would motivate consideration of the supernova and gas distributions inside a starburst.

We are pleased to thank Keith Bechtol for providing the Fermi data points, Wystan Benbow for providing VERITAS data points, Roger Blandford, Ellen Zweibel and Anne Sickles for the stimulating conversation. This work was supported in part by the NASA Astrophysics Theory Program through award NNX10AC86G.

A. Energy Loss Rates

The energy losses other than Pion process in our model are elastic scattering and ionization, they are expressed as follows (Gould 1982; Ginzburg & Syrovatskii 1964):

$$b_{\text{elastic,p}} \sim 2.44 \times 10^{-16} \frac{n_p}{\text{cm}^{-3}} \frac{E_p}{\text{GeV}} \left(\frac{E_p}{m_p c^2} \right)^{1/2} \frac{(1 + E_p/2m_p c^2)^{1/2}}{1 + E_p/m_p c^2} \text{GeV s}^{-1} \quad (\text{A1})$$

$$b_{\text{ionic,p}} \sim 1.83 \times 10^{-17} \left(\frac{n_{\text{H}} + 2n_{\text{H}_2}}{\text{cm}^{-3}} \right) \frac{c}{v_{\text{p}}} \left\{ 10.9 + 2 \ln \left(\frac{E_{\text{p}}}{m_{\text{p}} c^2} \right) + \ln \left(\frac{v_{\text{p}}^2}{c^2} \right) - \frac{v_{\text{p}}^2}{c^2} \right\} \text{GeV s}^{-1} \quad (\text{A2})$$

where n_{p} and $n_{\text{H}} + 2n_{\text{H}_2}$ are the number densities of protons in the ISM, which are equal to n_{gas} . Here, E_{p} is the total energy of a proton, T_{p} denotes kinetic energy of a proton. In GeV energy range, elastic scattering contributes about 50% lower than inelastic scattering does to the total energy-loss during CR propagation. Therefore it's necessary to include elastic scattering during the propagation.

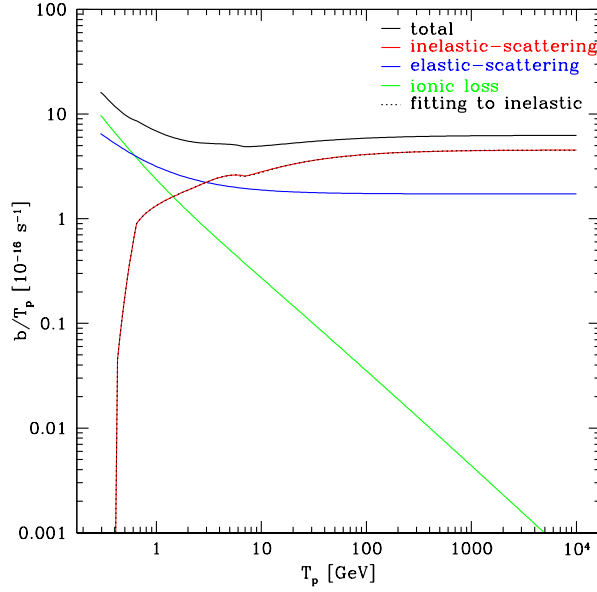


Fig. 8.— Energy Loss Rate Per Proton Kinetic Energy. The black line is the total energy loss rate per proton kinetic energy, blue line is elastic energy loss rate per proton kinetic energy, green line is ionic energy loss rate per proton kinetic energy, red line is inelastic (pionic) energy loss rate per proton kinetic energy, black dotted line is our fit curve to inelastic energy loss. Here $n_{\text{gas}} = 1 \text{ g/cm}^2$.

At high energy, $E_{\text{p}} \sim T_{\text{p}}$: As Fig. 8 shows, for $T_{\text{p}} > 100 \text{ GeV}$, $b(E_{\text{p}}) \propto E_{\text{p}}$, therefore, eq 6 gives $\phi_{\text{p}} \propto E_{\text{p}}^{-s}$; and for high T_{π} , $d\sigma_{\pi}(T_{\text{p}}, T_{\pi})/dT_{\pi} = \langle \zeta \sigma_{\pi}(T_{\text{p}}) \rangle dN(T_{\text{p}}, T_{\pi})/dT_{\pi} \propto 1/T_{\text{p}}$, we can get $q_{\pi} \propto E_{\pi}^{-s}$ from Eq 7 in § 2.2, thus $q_{\gamma} \propto E_{\gamma}^{-s}$, or $F_{\gamma} \propto E_{\gamma}^{-s}$. Therefore the gamma-ray spectrum obtained from our thick-target model has the same spectral index s as the injected proton's.

An analytical fit to our self-consistent inelastic energy loss appears is shown in Fig. 8 as the black dotted curve. The fit is good with fractional error less than 2% over the *Fermi* energy range.

The fitting function is:

$$\begin{aligned}
Y = & 0.631x^2 + 0.502x - 0.441, x_{\text{threshold}} \leq x \leq -0.24 \\
& -1.66x^2 - 0.605x - 0.575, -0.24 \leq x \leq -0.05 \\
& -0.430x - 0.568, -0.05 \leq x \leq 0.6 \\
& -0.643x - 0.440, 0.6 \leq x \leq 0.75 \\
& -0.157 \ln(x - 0.639) - 1.26, 0.75 \leq x \leq 1.10 \\
& -0.677 \ln(x + 0.817) - 0.701, 1.10 \leq x
\end{aligned} \tag{A3}$$

where $Y = \log_{10}(b_{\text{inelastic}}/\langle \zeta \sigma_{\pi}(X) \rangle)$ with $x = \log_{10}(T_p/1\text{GeV})$, $x_{\text{threshold}} = \log_{10}(T_p^{\text{min}}/1\text{GeV})$, for $n_{\text{gas}} = 1 \text{ g/cm}^2$.

B. Code Description

We build a simple code following the calculation in § 2, using the Simpson method to do integration and the relative errors for the integrations set to be 10^{-4} . Because the model is closed box, we can do conservation check of the code: $N_{\gamma} = 2N_{\pi} = 2N_p/3$ (number conservation), and $L_{\gamma} = L_{\pi} < L_p/3$ (energy conservation) (Kelner et al. 2006). The code results we get fulfill the conservation check. To reduce the CPU time taken for code running, instead of doing the 3-layer integration, we do the first 2-layer integration first to get the values of q_{π} vs. E_{π} and store them as vectors, then doing the third integration to get q_{γ} simply by doing interpolation and extrapolation to the stored values of q_{π} .

C. Nuclear Enhancement Factor

In the thick-target model, the gamma-ray flux is calculated by neutral pion decay which is produced through CR proton interacting with ISM proton. However, there are heavier nuclei both in cosmic-rays and ISM which can also produce neutral pions, bringing a nuclear enhancement factor \mathcal{A} to be multiplied to the gamma-ray yield assuming cosmic-ray protons on ISM protons only: $dq_{\gamma}^{\text{total}}/dE_{\gamma} = \mathcal{A}dq_{\gamma}^{\text{pp,only}}/E_{\gamma}$.

Assume all CR source ($i = p, \text{He}, \text{CNO}, \text{NeMgSiS}, \text{Fe}$) spectra have the same shape in energy per nucleon $\epsilon = E_i/A_i$.

$$y_i^{\text{CR}} = \frac{dq_i/d\epsilon}{dq_p/d\epsilon} \tag{C1}$$

$$\frac{dq_i}{d\epsilon} = y_i^{\text{CR}} \frac{dq_p}{d\epsilon} \tag{C2}$$

$$\frac{q_i}{q_p} = \frac{\int d\epsilon dq_i/d\epsilon}{\int d\epsilon dq_p/d\epsilon} = \frac{\int d\epsilon y_i^{\text{CR}} dq_p/d\epsilon}{\int d\epsilon dq_p/d\epsilon} = y_i^{\text{CR}} \tag{C3}$$

$$\begin{aligned}
L_i &= \int dV E_i q_i = \int dV \int E_i \frac{dq_i}{d\epsilon} d\epsilon \\
&= \int dV \int A_i \epsilon \frac{dq_i}{d\epsilon} d\epsilon \\
&= A_i y_i^{\text{CR}} \int dV \int \epsilon \frac{dq_p}{d\epsilon} d\epsilon \\
&= A_i y_i^{\text{CR}} L_p
\end{aligned} \tag{C4}$$

$$L_{\text{CR}} = \int dV \int \epsilon (dq_{\text{CR}}/d\epsilon) d\epsilon = \sum_i L_i = \sum_i A_i y_i^{\text{CR}} L_p \tag{C5}$$

$$\frac{dq_p}{d\epsilon} = \frac{1}{\sum_i A_i y_i^{\text{CR}}} \frac{dq_{\text{CR}}}{d\epsilon} \tag{C6}$$

$$\frac{q_p}{q_{\text{CR}}} = \frac{1}{\sum_i A_i y_i^{\text{CR}}} \tag{C7}$$

For a closed-box model,

$$\Phi_i = \frac{v_i}{b_i} \int \frac{dq_i}{d\epsilon} d\epsilon \tag{C8}$$

$$\frac{\Phi_i}{\Phi_p} = \frac{q_i}{q_p} \frac{b_p}{b_i} = y_i^{\text{CR}} \frac{b_p}{b_i} \tag{C9}$$

Assume energy loss is all nucleus-loss, then the total energy loss rate per nucleon for each source i is:

$$b_i = b_i^{\text{inelastic}} + b_i^{\text{elastic}} \tag{C10}$$

$$b_i^{\text{inelastic}} \propto \sum_j n_j \sigma_{ij}^{\text{inelastic}} \tag{C11}$$

$$b_i^{\text{elastic}} \propto \sum_j n_j \sigma_{ij}^{\text{elastic}} \tag{C12}$$

$$y_i^{\text{ISM}} = \frac{n_i}{n_p} \tag{C13}$$

$$b_i^{\text{inelastic}} = \sum_j y_j^{\text{ISM}} \frac{\sigma_{ij}^{\text{inelastic}}}{\sigma_{pp}^{\text{inelastic}}} b_{pp}^{\text{inelastic}} \tag{C14}$$

$$b_i^{\text{elastic}} = \sum_j y_j^{\text{ISM}} \frac{\sigma_{ij}^{\text{elastic}}}{\sigma_{pp}^{\text{elastic}}} b_{pp}^{\text{elastic}} \tag{C15}$$

Assume $\sigma_{ij}^{\text{inelastic}}/\sigma_{pp}^{\text{inelastic}} = \sigma_{ij}^{\text{elastic}}/\sigma_{pp}^{\text{elastic}} = \sigma_{ij}^t/\sigma_{pp}^t$, then we can get

$$b_i = b_{pp} \sum_j y_j^{\text{ISM}} \frac{\sigma_{ij}^t}{\sigma_{pp}^t} \quad (\text{C16})$$

$$b_p = b_{pp} \sum_i y_i^{\text{ISM}} \frac{\sigma_{pi}^t}{\sigma_{pp}^t} \quad (\text{C17})$$

Therefore

$$\frac{\Phi_i}{\Phi_p} = y_i^{\text{CR}} \frac{\sum_l y_l^{\text{ISM}} \sigma_{pl}^t / \sigma_{pp}^t}{\sum_j y_j^{\text{ISM}} \sigma_{ij}^t / \sigma_{pp}^t} \quad (\text{C18})$$

$$\frac{dq_{\gamma}^{ij}}{dE_{\gamma}} = 2 \int_{u(E_{\gamma})} \frac{dE_{\pi}}{p_{\pi}} \frac{dq_{\pi}^{ij}}{dE_{\pi}} = \int q_{\pi}^{ij} \quad (\text{C19})$$

$$\frac{dq_{\pi}^{ij}}{dE_{\pi}} = \int d\epsilon_i n_j \Phi_i \langle \zeta_{ij}^{\pi} \sigma_{ij}^{\pi} \rangle \frac{dN}{dE_{\pi}}(\epsilon_i, E_{\pi}) \quad (\text{C20})$$

$$\begin{aligned} dq_{\gamma}^{\text{total}}/dE_{\gamma} &= \int q_{\pi}^{\text{total}} = \int \sum_{i,j} q_{\pi}^{ij} = \int q_{\pi}^{\text{pp}} \sum_{i,j} q_{\pi}^{ij}/q_{\pi}^{\text{pp}} \\ &= \int q_{\pi}^{\text{pp}} \sum_{i,j} \frac{dq_{\pi}^{ij}/dE_{\pi}}{dq_{\pi}^{\text{pp}}/dE_{\pi}} = \int q_{\pi}^{\text{pp,only}} \mathcal{A} = \mathcal{A} \int q_{\pi}^{\text{pp,only}} \\ &= \mathcal{A} dq_{\gamma}^{\text{pp,only}}/dE_{\gamma} \end{aligned} \quad (\text{C21})$$

where \mathcal{A} is a number.

$$\begin{aligned} \sum_{i,j} \frac{dq_{\pi}^{ij}/dE_{\pi}}{dq_{\pi}^{\text{pp}}/dE_{\pi}} &= \sum_{i,j} y_j^{\text{ISM}} \frac{\Phi_i}{\Phi_p} \frac{\langle \zeta_{ij}^{\pi} \sigma_{ij}^{\pi} \rangle}{\langle \zeta_{pp}^{\pi} \sigma_{pp}^{\pi} \rangle} \\ &= \sum_{i,j} y_j^{\text{ISM}} \frac{\langle \zeta_{ij}^{\pi} \sigma_{ij}^{\pi} \rangle}{\langle \zeta_{pp}^{\pi} \sigma_{pp}^{\pi} \rangle} y_i^{\text{CR}} \frac{\sum_l y_l^{\text{ISM}} \sigma_{pl}^t / \sigma_{pp}^t}{\sum_k y_k^{\text{ISM}} \sigma_{ik}^t / \sigma_{pp}^t} \end{aligned} \quad (\text{C22})$$

$$q_{\pi}^{\text{pp}} \propto \frac{n_{\text{p}} \langle \zeta_{\text{pp}}^{\pi} \sigma_{\text{pp}}^{\pi} \rangle q_{\text{p}}}{b_{\text{p}}} \quad (\text{C23})$$

$$q_{\pi}^{\text{pp,only}} \propto \frac{n_{\text{p}} \langle \zeta_{\text{pp}}^{\pi} \sigma_{\text{pp}}^{\pi} \rangle q_{\text{CR}}}{b_{\text{pp}}} \quad (\text{C24})$$

$$q_{\pi}^{\text{pp}} = q_{\pi}^{\text{pp,only}} \frac{q_{\text{p}}}{q_{\text{CR}}} \frac{b_{\text{pp}}}{b_{\text{p}}} = q_{\pi}^{\text{pp,only}} \frac{1}{\sum_i A_i y_i^{\text{CR}}} \frac{1}{\sum_i y_i^{\text{ISM}} \sigma_{\text{pi}}^{\text{t}} / \sigma_{\text{pp}}^{\text{t}}} \quad (\text{C25})$$

therefore

$$\begin{aligned} \mathcal{A} &= \frac{q_{\pi}^{\text{pp}}}{q_{\pi}^{\text{pp,only}}} \sum_{i,j} \frac{dq_{\pi}^{\text{ij}}/dE_{\pi}}{dq_{\pi}^{\text{pp}}/dE_{\pi}} \\ &= \frac{1}{\sum_i A_i y_i^{\text{CR}}} \frac{1}{\sum_i y_i^{\text{ISM}} \sigma_{\text{pi}}^{\text{t}} / \sigma_{\text{pp}}^{\text{t}}} \sum_{i,j} y_j^{\text{ISM}} \frac{\langle \zeta_{\text{ij}}^{\pi} \sigma_{\text{ij}}^{\pi} \rangle}{\langle \zeta_{\text{pp}}^{\pi} \sigma_{\text{pp}}^{\pi} \rangle} y_i^{\text{CR}} \frac{\sum_l y_l^{\text{ISM}} \sigma_{\text{pl}}^{\text{t}} / \sigma_{\text{pp}}^{\text{t}}}{\sum_k y_k^{\text{ISM}} \sigma_{\text{ik}}^{\text{t}} / \sigma_{\text{pp}}^{\text{t}}} \\ &= \frac{1}{\sum_i A_i y_i^{\text{CR}}} \frac{1}{\sum_i y_i^{\text{ISM}} \sigma_{\text{pi}}^{\text{t}} / \sigma_{\text{pp}}^{\text{t}}} \left(\sum_l y_l^{\text{ISM}} \frac{\sigma_{\text{pl}}^{\text{t}}}{\sigma_{\text{pp}}^{\text{t}}} \right) \frac{\sum_i y_i^{\text{CR}} \sum_j y_j^{\text{ISM}} \langle \zeta_{\text{ij}}^{\pi} \sigma_{\text{ij}}^{\pi} \rangle / \langle \zeta_{\text{pp}}^{\pi} \sigma_{\text{pp}}^{\pi} \rangle}{\sum_k y_k^{\text{ISM}} \sigma_{\text{ik}}^{\text{t}} / \sigma_{\text{pp}}^{\text{t}}} \quad (\text{C26}) \end{aligned}$$

As discussed in Abbott et al. (1992); Miller et al. (2007), the total multiplicity $R_{\text{ij}}^{\pi^0}$ for making π^0 through collision of nuclei $i+j$ is almost universal, i.e., $R_{\text{ij}}^{\pi^0} = \langle \zeta_{\text{ij}}^{\pi} \sigma_{\text{ij}}^{\pi} \rangle / \sigma_{\text{ij}}^{\text{inelastic}} = R_{\text{pp}}^{\pi} = \text{constant}$, thus it's safe to assume $\langle \zeta_{\text{ij}}^{\pi} \sigma_{\text{ij}}^{\pi} \rangle / \langle \zeta_{\text{pp}}^{\pi} \sigma_{\text{pp}}^{\pi} \rangle = \sigma_{\text{ij}}^{\text{t}} / \sigma_{\text{pp}}^{\text{t}}$ for all energy per nucleon ϵ for CR nuclei i interact with ISM nuclei j , then we can get:

$$\begin{aligned} \mathcal{A} &= \frac{1}{\sum_i A_i y_i^{\text{CR}}} \frac{1}{\sum_i y_i^{\text{ISM}} \sigma_{\text{pi}}^{\text{t}} / \sigma_{\text{pp}}^{\text{t}}} \left(\sum_l y_l^{\text{ISM}} \frac{\sigma_{\text{pl}}^{\text{t}}}{\sigma_{\text{pp}}^{\text{t}}} \right) \left(\sum_i y_i^{\text{CR}} \right) \\ &= \frac{1}{\sum_i A_i y_i^{\text{CR}}} \sum_i y_i^{\text{CR}} \\ &= \frac{1}{\langle A \rangle_{\text{CR}}} \quad (\text{C27}) \end{aligned}$$

Considering the same heavier nuclei components in both CR and ISM as Mori (2009) did, if use the relative abundance of H : He : CNO : NeMgSiS : Fe = 1:0.153:1.245 $\times 10^{-2}$:3.65 $\times 10^{-3}$:1.182 $\times 10^{-3}$ in Meyer (1985), the nuclear enhancement factor is $\mathcal{A} = 0.59$.

REFERENCES

Aartsen, M. G., Ackermann, M., Adams, J., et al. 2014, arXiv:1405.5303

- Abbott, T., Akiba, Y., Beavis, D., et al. 1992, *Phys. Rev. D*, 45, 3906
- Abdo, A. A., Ackermann, M., Ajello, M., et al. 2009, *Physical Review Letters*, 103, 251101
- Abdo, A. A., Ackermann, M., Ajello, M., et al. 2010, *A&A*, 512, A7
- Abdo, A. A., Ackermann, M., Ajello, M., et al. 2010, *A&A*, 523, A46
- Abdo, A. A., Ackermann, M., Ajello, M., et al. 2010, *A&A*, 523, L2
- Abdo, A. A., Ackermann, M., Ajello, M., et al. 2010, *ApJ*, 709, L152
- Abdo, A. A., Ackermann, M., Ajello, M., et al. 2010, *A&A*, 523, AA46
- Abdo, A. A., Ackermann, M., Ajello, M., et al. 2010, *A&A*, 512, AA7
- Abdo, A. A., Ackermann, M., Ajello, M., et al. 2010, *A&A*, 523, LL2
- Abramowski, A., Acero, F., Aharonian, F., et al. 2012, *ApJ*, 757, 158
- Acciari, V. A., Aliu, E., Arlen, T., et al. 2009, *Nature*, 462, 770
- Acero, F., Aharonian, F., Akhperjanian, A. G., et al. 2009, *Science*, 326, 1080
- Acero, F., Ackermann, M., Ajello, M., et al. 2015, *arXiv:1511.06778*
- Ackermann, M., Ajello, M., Allafort, A., et al. 2012, *ApJ*, 755, 164
- Ackermann, M., Ajello, M., Allafort, A., et al. 2013, *Science*, 339, 807
- Aharonian, F., Akhperjanian, A. G., Bazer-Bachi, A. R., et al. 2005, *A&A*, 441, 465
- Aharonian, F., Akhperjanian, A. G., Bazer-Bachi, A. R., et al. 2008, *A&A*, 481, 401
- Ahlers, M., & Murase, K. 2013, *arXiv:1309.4077*
- Aliu, E., Archambault, S., Arlen, T., et al. 2013, *ApJ*, 764, 38
- Anchordoqui, L. A., Goldberg, H., Halzen, F., & Weiler, T. J. 2004, *Physics Letters B*, 600, 202
- Baade, W., & Zwicky, F. 1934, *Proceedings of the National Academy of Science*, 20, 259
- Bell, A. R. 1978, *MNRAS*, 182, 147
- Blandford, R. D., & Ostriker, J. P. 1978, *ApJ*, 221, L29
- Blasi, P., & Amato, E. 2012, *J. Cosmology Astropart. Phys.*, 1, 10
- Blasi, P. 2013, *A&A Rev.*, 21, 70
- Blom, J. J., Paglione, T. A. D., & Carramiñana, A. 1999, *ApJ*, 516, 744

- Brun, F., de Naurois, M., Hofmann, W., et al. 2011, arXiv:1104.5003
- Caprioli, D. 2012, *J. Cosmology Astropart. Phys.*, 7, 38
- Chabrier, G. 2003, *PASP*, 115, 763
- Chang, X.-C., & Wang, X.-Y. 2014, arXiv:1406.1099
- de Cea del Pozo, E., Torres, D. F., & Rodriguez Marrero, A. Y. 2009, *ApJ*, 698, 1054
- Dermer, C. D. 1986, *A&A*, 157, 223
- Dermer, C. D., Strong, A. W., Orlando, E., Tibaldo, L., & for the Fermi Collaboration 2013, arXiv:1307.0497
- Dermer, C. D., & Powale, G. 2013, *A&A*, 553, A34
- Domingo-Santamaría, E., & Torres, D. F. 2005, *A&A*, 444, 403
- Downes, D., & Eckart, A. 2007, *A&A*, 468, L57
- Eichmann, B., & Becker Tjus, J. 2016, *ApJ*, 821, 87
- Evoli, C., Gaggero, D., Grasso, D., & Maccione, L. 2008, *J. Cosmology Astropart. Phys.*, 10, 18
- Fleischhack, H., & for the VERITAS collaboration 2015, arXiv:1508.05807
- Fields, B. D., Olive, K. A., & Schramm, D. N. 1994, *ApJ*, 435, 185
- Fields, B. D., Olive, K. A., Cassé, M., & Vangioni-Flam, E. 2001, *A&A*, 370, 623
- Fields, B. D., Pavlidou, V., & Prodanović, T. 2010, *ApJ*, 722, L199
- Fox, O. D., & Casper, C. 2015, *IAU General Assembly*, 22, 2258045
- Gao, Y., & Solomon, P. M. 2004, *ApJ*, 606, 271
- Ginzburg, V. L., & Syrovatskii, S. I. 1964, *The Origin of Cosmic Rays*, New York: Macmillan, 1964
- Gould, R. J. 1982, *ApJ*, 263, 879
- Griffin, R. D., Dai, X., & Thompson, T. A. 2016, *ApJ*, 823, L17
- Halzen, F., & Hooper, D. 2002, *Reports on Progress in Physics*, 65, 1025
- Hassan, T., Arrabito, L., Bernlör, K., et al. 2015, arXiv:1508.06075
- Hayakawa, S. 1969, *Interscience Monographs and Texts in Physics and Astronomy*, New York: Wiley-Interscience, 1969

- Hayashida, M., Stawarz, L., Cheung, C. C., et al. 2013, arXiv:1310.1913
- Horiuchi, S., Beacom, J. F., & Dwek, E. 2009, Phys. Rev. D, 79, 083013
- Horiuchi, S., Beacom, J. F., Kochanek, C. S., et al. 2011, ApJ, 738, 154
- IceCube Collaboration, Aartsen, M. G., Ackermann, M., et al. 2014, arXiv:1406.6757
- Kamae, T., Karlsson, N., Mizuno, T., Abe, T., & Koi, T. 2006, ApJ, 647, 692
- Kang, H., Jones, T. W., & Edmon, P. P. 2013, ApJ, 777, 25
- Kelner, S. R., Aharonian, F. A., & Bugayov, V. V. 2006, Phys. Rev. D, 74, 034018
- Kennicutt, R. C., Jr. 1998, ApJ, 498, 541
- Krymskii, G. F. 1977, Akademiia Nauk SSSR Doklady, 234, 1306
- Lacki, B. C., Thompson, T. A., & Quataert, E. 2010, ApJ, 717, 1
- Lacki, B. C., Thompson, T. A., Quataert, E., Loeb, A., & Waxman, E. 2011, ApJ, 734, 107
- Lacki, B. C., Horiuchi, S., & Beacom, J. F. 2012, arXiv:1206.0772
- Lacki, B. C., & Thompson, T. A. 2013, ApJ, 762, 29
- Lemoine-Goumard, M., Renaud, M., Vink, J., et al. 2012, A&A, 545, A28
- Lichti, G. G., Bignami, G. F., & Paul, J. A. 1978, Ap&SS, 56, 403
- Lien, A., & Fields, B. D. 2009, J. Cosmology Astropart. Phys., 1, 47
- Loeb, A., & Waxman, E. 2006, J. Cosmology Astropart. Phys., 5, 3
- Longair, M. S. 1981, Cambridge and New York, Cambridge University Press, 1981. 420 p.,
- Meneguzzi, M., Audouze, J., & Reeves, H. 1971, A&A, 15, 337
- Meyer, J.-P. 1985, ApJS, 57, 173
- Miller, M. L., Reygers, K., Sanders, S. J., & Steinberg, P. 2007, Annual Review of Nuclear and Particle Science, 57, 205
- Morlino, G., & Caprioli, D. 2012, A&A, 538, A81
- Morlino, G., & Blasi, P. 2015, arXiv:1511.05343
- Mori, M. 2009, Astroparticle Physics, 31, 341
- Murase, K., Ahlers, M., & Lacki, B. C. 2013, Phys. Rev. D, 88, 121301

- Nolan, P. L., Abdo, A. A., Ackermann, M., et al. 2012, *ApJS*, 199, 31
- Ohm, S. 2016, *Comptes Rendus Physique*, 17, 585
- Olive, K. A., & Particle Data Group 2014, *Chinese Physics C*, 38, 090001
- Paglione, T. A. D., Marscher, A. P., Jackson, J. M., & Bertsch, D. L. 1996, *ApJ*, 460, 295
- Paglione, T. A. D., & Abrahams, R. D. 2012, *ApJ*, 755, 106
- Pavlidou, V., & Fields, B. D. 2001, *ApJ*, 558, 63
- Peng, F.-K., Wang, X.-Y., Liu, R.-Y., Tang, Q.-W., & Wang, J.-F. 2016, *ApJ*, 821, L20
- Persic, M., Rephaeli, Y., & Arieli, Y. 2008, *A&A*, 486, 143
- Planck Collaboration, Ade, P. A. R., Aghanim, N., et al. 2015, *arXiv:1502.01589*
- Pohl, M. 1993, *A&A*, 270, 91
- Pohl, M. 1994, *A&A*, 287, 453
- Rephaeli, Y., Arieli, Y., & Persic, M. 2010, *MNRAS*, 401, 473
- Sakamoto, K., Wang, J., Wiedner, M. C., et al. 2008, *ApJ*, 684, 957-977
- Salamon, M. H., & Stecker, F. W. 1998, *ApJ*, 493, 547
- Sanders, D. B., Mazzeella, J. M., Kim, D.-C., Surace, J. A., & Soifer, B. T. 2003, *AJ*, 126, 1607
- Slane, P., Lee, S.-H., Ellison, D. C., et al. 2014, *ApJ*, 783, 33
- Stecker, F. W. 1970, *Ap&SS*, 6, 377
- Stecker, F. W. 1971, *NASA Special Publication*, 249
- Stecker, F. W., & Venters, T. M. 2011, *ApJ*, 736, 40
- Stecker, F. W., Malkan, M. A., & Scully, S. T. 2012, *ApJ*, 761, 128
- Stephens, S. A., & Badhwar, G. D. 1981, *Ap&SS*, 76, 213
- Strong, A. W., Wolfendale, A. W., & Worrall, D. M. 1976, *MNRAS*, 175, 23P
- Strong, A. W., & Moskalenko, I. V. 1998, *ApJ*, 509, 212
- Strong, A. W., Moskalenko, I. V., & Ptuskin, V. S. 2007, *Annual Review of Nuclear and Particle Science*, 57, 285
- Strong, A. W., Porter, T. A., Digel, S. W., et al. 2010, *ApJ*, 722, L58

- Torres, D. F. 2004, *ApJ*, 617, 966
- Torres, D. F., Reimer, O., Domingo-Santamaría, E., & Digel, S. W. 2004, *ApJ*, 607, L99
- Tully, R. B., Rizzi, L., Shaya, E. J., et al. 2009, *AJ*, 138, 323
- Tunnard, R., Greve, T. R., Garcia-Burillo, S., et al. 2015, *ApJ*, 800, 25
- Voelk, H. J. 1989, *A&A*, 218, 67
- Wang, X., & Fields, B. D. 2014, *American Institute of Physics Conference Series*, 1595, 231
- Wang, X., & Fields, B. D. 2016, *PoS ICRC* **2015**, 905 (2016).
- Wik, D. R., Lehmer, B. D., Hornschemeier, A. E., et al. 2014, *ApJ*, 797, 79
- Wilson, C. D., Rangwala, N., Glenn, J., et al. 2014, *ApJ*, 789, L36
- Woosley, S. E., & Weaver, T. A. 1995, *ApJS*, 101, 181
- Yoast-Hull, T. M., Everett, J. E., Gallagher, J. S., III, & Zweibel, E. G. 2013, *ApJ*, 768, 53
- Yoast-Hull, T. M., Gallagher, J. S., III, Zweibel, E. G., & Everett, J. E. 2014, *ApJ*, 780, 137
- Yoast-Hull, T. M., Gallagher, J. S., & Zweibel, E. G. 2015, *MNRAS*, 453, 222